Polymeric Electro-optic Modulators: From Chromophore Design to Integration with Semiconductor Very Large Scale Integration Electronics and Silica Fiber Optics

L. Dalton, A. Harper, A. Ren, F. Wang, G. Todorova, J. Chen, C. Zhang, and M. Lee

Loker Hydrocarbon Research Institute, University of Southern California, Los Angeles, California 90089-1661

Chromophores with optimized second-order optical nonlinearity to optical loss ratios are synthesized, poled with an electrical field, and coupled into hardened polymer matrixes. Acentric order, which is necessary for electro-optic activity, is optimized by the consideration of chromophore−chromophore electrostatic interactions as well as chromophore−poling field interactions and thermal collisions which randomize chromophore orientations with respect to the applied field direction. Reactive ion etching and/or multicolor photolithography are used to fabricate buried channel waveguide structures out of the resulting polymeric electro-optic materials and to integrate polymeric waveguides with silica optical fibers. Tapered transitions are developed to minimize coupling (insertion) loss. Both vertical and horizontal integration of polymeric electro-optic modulator circuitry with semiconductor very large scale integration circuitry is demonstrated. Modulation to 113 GHz is demonstrated. Polymeric modulators are relevant to cable television, phased-array radar, ultrafast analogue-to-digital conversion, high-speed optical switching in local area networks, optical beam steering, optical backplane interconnects for parallel processors, and voltage sensing.

1. Introduction

1.1. The Phenomenon of Electro-optic Activity and Its Applications. An applied electric field (0−120 GHz) perturbs the electron distribution of a material affecting the transit of light through the material. The result is an electric field dependent change in the index of refraction of the material and phase shift of light.

For a significant perturbation of light (e.g., a phase shift of one-half a wavelength, π) to be realized with the application of small applied voltages, the electrons of the material must be weakly confined by the nuclei (i.e., the electrons must be highly polarizable). For organic materials, π-electrons are much less tightly bound by nuclei than σ-electrons as is easily understood from considering their relative positioning with respect to nuclei. Thus, more than 2 decades ago, π-electron organic materials were identified as promising candidates for nonlinear optical applications.[1,2]

A field-dependent index of refraction can be utilized to achieve electrical-to-optical signal transduction (e.g., as in the cable television (CATV) industry), optical switching (e.g., at nodes in local area optical networks, LANs), and small-angle beam steering (e.g., for addressing phosphors in flat panel displays). Electro-optic modulators may well be one of the most critical hardware components of the information superhighway.

Electro-optic activity is one example of second-order nonlinear optical activity (the activity associated with the quadratic term in the power series expansion of polarization in terms of an applied electric field).[1−3] Another example of second-order optical nonlinearity is second harmonic generation or frequency doubling. Third-order optical nonlinearity, leading to optical rectification, phase conjugation, third harmonic generation, and the Kerr effect, is also of considerable interest but will not be discussed here.[1−3] Typically, and as expected for a power series expansion, third-order coefficients are sufficiently smaller than second-order effects as to make their application impossible except for situations involving very long interaction lengths of material.

1.2. Why Organic Materials? Quantum mechanical calculations have long predicted large molecular hyperpolarizabilities for π-electron organic chromophores.[1,2,4−6] If such chromophores could be assembled into stable acentric lattices, then large molecular first hyperpolarizabilities, β, could be translated into macroscopic material electro-optic activity (electro-optic coefficients, r). Such large electro-optic coefficients would, in turn, permit π-phase shifts (required for full wave modulation or complete optical switching) to be achieved with digital level (less than 6 V) drive voltages, V_π. Since the fastest semiconductor electronics operate with digital level voltages (and increasingly with voltages approaching 1 V), this drive voltage requirement is critical for the production of integrated optoelectronic circuits such as those required for optical switching in LANs, ultrafast A/D conversion, and ultrafast electrical-to-optical signal transduction. Lithium niobate, the current most commonly used electro-optic material, has an electro-optic coefficient of 35 pm/V which permits V_π voltages on the order of 5 V to be reasonably achieved. For organic materials to compete with lithium niobate for use in low V_π devices (e.g., those to be directly integrated with low-voltage very large scale integration (VLSI) semiconductor circuits avoiding the use of additional voltage amplifiers), the electro-optic coefficients must equal or exceed that of lithium niobate. However, as we shall shortly discuss, organics have other advantages which may make them preferable to lithium niobate for certain applications even if the electro-optic coefficients are only a fraction (e.g., $^1/_2$ or $^1/_3$) of that of lithium niobate.

The low dielectric constants (approximately 3) of organic materials permit large (e.g., greater than 120 GHz for a 1 cm device) bandwidths to be achieved. It is

10.1021/ie9705970 CCC: $18.00
Published on Web 12/12/1998

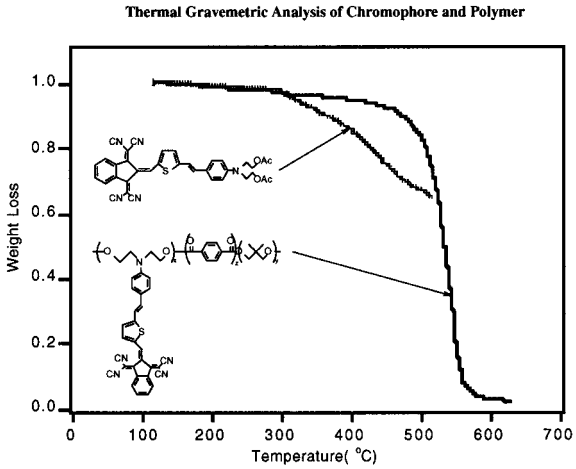

Figure 1. The thermogravimetric analysis of a tetracyanoindane, TCI, chromophore (see Table 1) is shown both neat and covalently incorporated into a polymer matrix.

desirable for the applied electrical and optical waves to copropagate at the same velocity in a nonlinear optical material waveguide so that their interaction length is long. Since the index of refraction (which determines optical wave velocity) and dielectric constant (which determines electrical wave velocity) are both defined by the π-electrons of organic materials, the two waves can travel significant (centimeter) distances without dephasing. This long interaction length also permits the drive voltage to be minimized. A lithium niobate device of comparable dimensions (e.g., 1 cm) exhibits a bandwidth of less than 10 GHz. However, it can be noted that, by clever device design, lithium niobate modulators have been demonstrated up to 90 GHz but with reduced modulation efficiency (i.e., increased drive voltage requirements).

The final putative advantage of polymeric organic materials is their ease of processability which should permit easier integration with semiconductor very large scale integration (VLSI) electronics than can be achieved with crystalline materials such as lithium niobate which currently requires exotic connections such as flip chip bonding.[7] Spin casting of thin films should be appropriate for most polymeric electro-optic materials.

1.3. Issues To Be Addressed in the Fabrication of Polymeric EO Modulators. First of all, chromophores must be synthesized with large molecular hyperpolarizability and low optical absorption at the intended operational wavelength (e.g., the communication wavelengths of 1.3 and 1.55 μm or diode laser wavelengths of 820−980 nm). Chromophores must be capable of being incorporated into polymer lattices and must be chemically and thermally robust to withstand subsequent processing and device operating conditions. As shown in Figure 1, thermal stability can conveniently be assessed by standard thermal gravimetric analysis (TGA) and differential scanning calorimetry (DSC) methods.

Chromophores must be assembled into an acentric lattice to translate molecular optical nonlinearity to macroscopic optical nonlinearity. This has been accomplished by molecular self-assembly (crystal growth, inclusion compounds, phase-separating block copolymers, etc.), sequential synthesis (quasi-epitaxy, Langmuir−Blodgett methods, and Merrifield methods), and by external field (electrical and laser) poling.[1,8,9] Of these approaches, external field poling is the most commonly used method of preparing materials for prototype device fabrication. Of the external electric field poling methods (corona, in-plane electrode, or parallel plate electrode poling), corona poling is perhaps the most commonly used. Thermal effects, which tend to randomize chromophore orientations, and chromophore−chromophore electrostatic interactions, which overall promote centric order, oppose electric field induced acentric order. Of course, poling-induced order must be achieved without the introduction of optical loss because of surface damage of the films or the introduction of material inhomogeneity.

Once an acentric chromophore order is induced, it must be stabilized to withstand subsequent material processing and electro-optic modulator device operation. Lattice hardening typically involves chemical coupling of both ends of the chromophore to a three-dimensional cross-linked polymer lattice. The precise thermal stability required for an electro-optic material depends on the particular application for which the material will be used. This can typically range from on the order of 100 °C to greater than 200 °C. Military specifications and applications that involve the fabrication of semiconductors on top of polymeric electro-optic modulator circuits typically require the latter. As with electric field poling, care must be exercised so that lattice hardening does not result in increased optical loss. Lattice hardening is an important issue in minimizing optical loss associated with reactive ion pitting during corona poling and solvent-pitting during deposition of a cladding layer onto the active core layer. Indeed, various processing steps can influence the outcome of other steps, and simple focus upon one process invariably leads to an inferior end device.

Once a hardened electro-optic material has been prepared, reactive ion etching or photolithography must be employed to fabricate buried-channel, electro-optic waveguides. Such waveguides must be developed without significant optical loss due to waveguide wall surface roughness. Polymer EO waveguides must be, at the very minimum, integrated with metal drive electrodes (to supply an electric voltage), a light source (to supply an optical carrier signal), and an output device such as an optical fiber or detector (to detect the modulation). Cladding layers must be added to shield light propagating in the active core (electro-optic waveguide) from the lossy metal electrodes. Issues such as matching the electrical conductivities and dielectric constants of the active core and cladding must be addressed. Device applications frequently require sophisticated integration with semiconductor VLSI electronics and silica fiber optical transmission lines and, in particular, the integration of many modulators in a single package. Again, integration must be accomplished without the introduction of significant optical loss. Finally, device performance must be evaluated over significant periods of time under environmentally relevant conditions.

Clearly, the fabrication and integration of polymeric electro-optic modulators requires that a substantial number of problems in materials science and device engineering be solved. Given the materials requirements which must be satisfied for device commercialization and given the complexity and demands of the materials processing protocols which must be satisfied to produce useful materials, it is surprising that polymeric electro-optic modulator materials are progressing

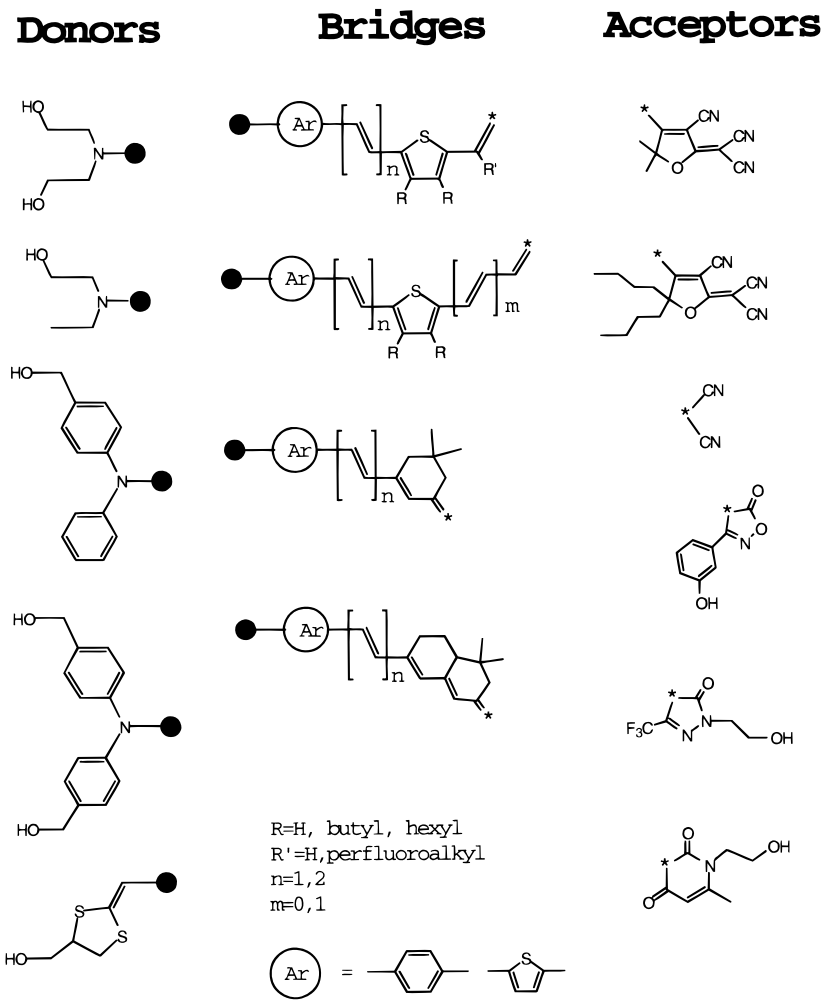

Figure 2. Representative donor, bridge, and acceptor segments are shown for dipolar (charge-transfer) second-order nonlinear optical chromophores.

to commercialization after a relatively short developmental period.

1.4. The Scope of this Article. It is to be emphasized that this article is not intended to be a comprehensive review of the organic electro-optic materials literature, which has now grown to many thousands of articles. For more detailed information, the reader is referred to the reviews cited in this article.[1−3,8,9] This article rather aims to acquaint the reader with critical concepts which have defined the progress of organic electro-optic materials evolving from laboratory curiosities to potential commercial devices and which guide the reader to anticipate future research directions and applications.

2. Chromophore Design and Synthesis

Second-order nonlinear optical chromophores have most commonly been dipolar (charge-transfer) chromophores consisting of donor, π-electron bridge, and acceptor segments as shown in Figure 2. Molecular hyperpolarizability, β, for such chromophores is well-described by quantum mechanical calculations, including two state calculations which predict that β is given by[1]

$$\beta = (\mu_{ee} - \mu_{gg})(\mu_{ge})^2/(E_{ge})^2 \qquad (1)$$

where $\mu_{ee} - \mu_{gg}$ is the difference between excited and ground-state dipole moments, μ_{ge} is the transition dipole moment, and E_{ge} is the optical (HOMO−LUMO) gap. Marder and co-workers[10] have not only verified the validity of this relationship but also adapted the relationship to the intuitive language of organic chemists as shown in Figure 3. Equation 1 indicates that there will be a sinusoidal relationship between β and the bond length alternation (or E_{ge}) with a value of zero realized for β when $E_{ge} = 0$ (zero bond length alternation). The conjugation of alkyl and aryl amine donor groups with phenyl and thienyl polyene bridge segments can be reasoned to shift the bond length alternation as shown in Figure 3 and thus result in the predicted variation in β recently verified by Marder and co-workers.[10]

Other empirical correlations can also be developed. For chromophores which contain organic acid acceptor groups, a correlation can be developed between the molecular hyperpolarizability β and the pK_a of the organic acid acceptor.[11]

Organic chemists have been very successful in producing ever-improved chromophores as can be seen from a consideration of Table 1. In 1990, disperse red (4,4′-aminonitroazobenzene) and (4,4′-aminonitrostilbene, DANS) chromophores represented state-of-the-art nonlinear optical chromophores. Since that time, hundreds of chromophores have been synthesized, dramatically exceeding the optical nonlinearity of those chromophores. If these new "high $\mu\beta$" chromophores (where μ is the chromophore ground-state dipole moment) could be

Table 1. Representative Electro-optic Chromophores with $\mu\beta$ Values (@ 1.9 mm, $\times 10^{-48}$ esu)

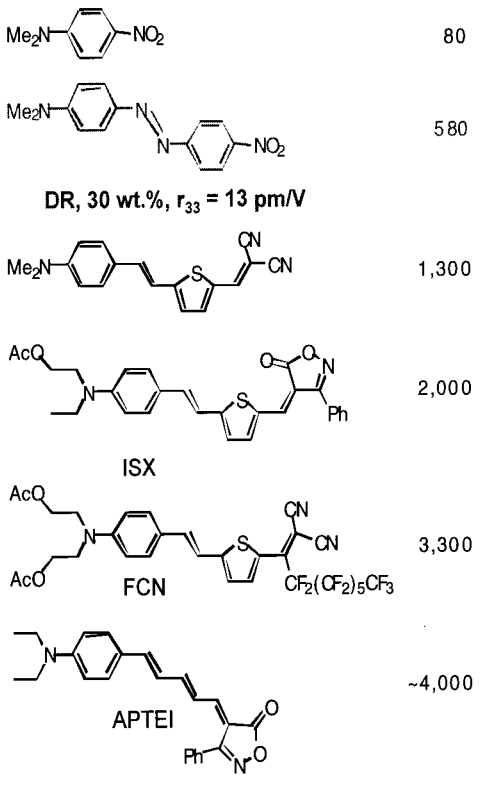

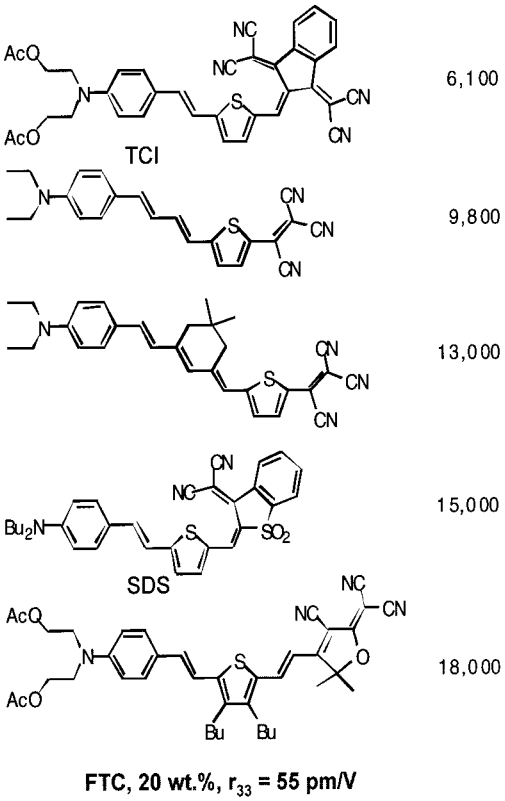

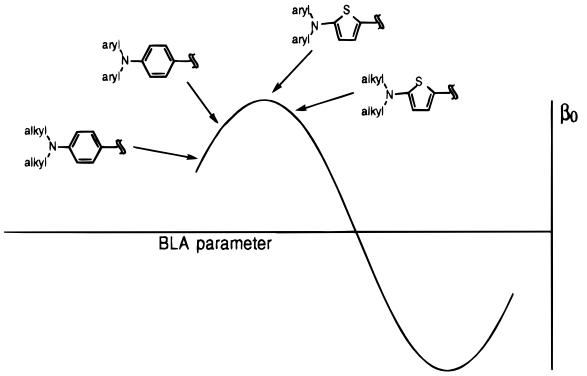

Figure 3. The variation of molecular first hyperpolarizability, β, with bond length alternation (BLA) is shown. The positioning of several representative chromophores along the theoretical curve is indicated. Chemical intuition argues that phenyl groups result in a greater bond length alternation than thiophene groups, etc.

incorporated into thermally stable polymer lattices with the same degree of loading and the same poling efficiency as achieved for disperse red and DANS chromophores, then electro-optic coefficients much larger than that of lithium niobate would be obtained.

Chromophore first hyperpolarizability, β, is characterized by techniques such as electric field induced second harmonic generation (EFISH)[12] and hyper-Rayleigh scattering (HRS),[13] although it should be noted that EFISH measures $\mu\beta$ rather than β and caution must be exercised with HRS as two-photon effects can lead to artificially high values of β. Results of HRS and EFISH, together with thermal (TGA and DSC) measurements, are given in Table 2 for a representative high $\mu\beta$ chromophore which we denote FTC (2-dicyanomethylen-3-cyano-4-{2-[*E*-(4-*N*,*N*-di(2-acetoxyethyl)amino)-phenylene-(3,4-dibutyl)thien-5]-*E*-vinyl}-5,5-dimethyl-2,5-dihydrofuran). Even higher $\mu\beta$ values have been

Table 2. Optical and Thermal Data for the FTC Chromophore

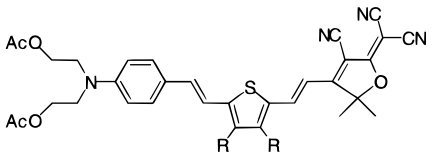

R = H, Bu

FTC

- μ = 13 D
- $\beta_0 = 635 \times 10^{-30}$ esu (HRS)
- $\mu\beta_{1.9\mu m} = 17{,}600 \times 10^{-48}$ esu (EFISH)
- T_d = 312 °C (DSC, 10 °C/min)
  315 °C (TGA, 10 °C/min)
- λ_{max} = 618 nm in dioxane
  650 nm in $CHCl_3$

obtained for the analogue of this chromophore where the phenylthienylvinylene bridge has been replaced by a isophorone-protected polyene bridge, but this greater molecular optical nonlinearity is realized with some sacrifice of thermal stability and red-shifting of the interband optical absorption (see Table 3).

Of course, other requirements such as low optical absorption at operating wavelengths (e.g., 980, 1300, and 1550 nm) and stability (thermal, chemical, and photochemical) must be satisfied by a chromophore before it can be considered as potentially useful for electro-optic applications. The FTC chromophore of Table 2 illustrates the type of parameters that characterize a chromophore with high potential for use as an electro-optic modulator material. Its thermal and photochemical stability are among the highest for any

Table 3. Comparison of Optical Nonlinearity and Thermal Stability for Second-Order Nonlinear Optical Chromophores

λ_{max} (nm)	$\mu\beta$ (10^{-48} esu)	Td (°C)
502	----	236
532	----	237
612	-----	195
585	5,600	203
600	3,300	274
595	3,300	-----
587	-----	-----
570	-----	260
650	17,600	312
648	~17,600	310
695	~35,000	271

Table 4. Comparison of High Thermal Stability Chromophores[a]

T_d (°C)	$\mu\beta_{1.9mm}$ (10^{-48} esu)
274	6200
296	2700
325	2500
354	1300
268	2520
322	1211
313	1720
367	2570

[a] Zhang and Jen et al. *Proc. SPIE* **1997**, *3006*, 372. Ermer et al. *Chem. Mater.* **1997**, *9*, 1498.

chromophore while, at the same time, the FTC chromopore exhibits exceptional hyperpolarizability and modest optical absorption at 1.3 and 1.55 μm. This chromophore, of course, would not be a chromophore of choice for applications at 980 nm or shorter wavelengths.

A comparison of chromophores designed primarily for high thermal stability is given in Table 4. To achieve a thermal stability (defined by TGA/DSC determined decomposition temperature T_d) greater than 300 °C typically limits optical nonlinearity (defined by $\mu\beta$) to less than 3000×10^{-48} esu. The FTC chromophore with a functionalized furan acceptor group is an obvious exception (see Tables 2 and 3). Table 4 is illustrative of the role of substitution of the cyanovinyl moiety in defining both chemical reactivity at elevated temperatures and optical nonlinearity. This once again illustrates the folly of choosing an acceptor functionality simply for maximum electron-withdrawing strength.

3. Generation of Acentric Chromophore Lattices

Once a chromophore characterized by an acceptable optical nonlinearity/absorption ratio and adequate stability has been identified, it must be organized into an acentric (noncentrosymmetric) lattice. This has been accomplished by a variety of molecular self-assembly and sequential synthesis methods including Langmuir−Blodgett film fabrication, molecular beam quasi-epitaxy (chemical vapor deposition), Merrifield-type sequential synthesis, crystal growth, incorporation into inclusion compounds, acentrically assembling block copolymer phases, etc.[1,8,9] However, these methods have yet to compete successfully on a routine basis with electric field poling as a method of inducing an acceptable degree of acentric order and it has been this latter approach which has routinely been used in the fabrication of prototype devices. Laser-assisted electric field poling[1] and all-optical poling[1] have also been introduced but again have not been widely used in the fabrication of devices.

Because the focus of this article is on the production of prototype devices, attention will now be directed to creating acentric lattices by various electric field poling techniques including use of corona, in-plane electrode, and coplanar electrode poling configurations. Before we begin a detailed discussion of poling, it is useful to review some theoretical concepts and the status of the field as of 1995.

For dipolar chromophores and electric field poling, the electro-optic coefficient, r, can be related to molecular first hyperpolarizability, β, by

$$r = 2N\beta f(\omega)\langle\cos^3\theta\rangle/n^4 \qquad (2)$$

where N = the chromophore number density, n = the index of refraction, and $f(\omega)$ = the product of local field (Debye) factors. The electric field induced acentric order parameter, $\langle\cos^3\theta\rangle$, can be computed from a knowledge of all forces affecting order using the Gibbs distribution function formalism (or the statistical mechanical partition function).

$$\langle\cos^3\theta\rangle = \int\cos^3\theta G(\Omega,E_p)\,d\Omega/\int G(\Omega,E_p)\,d\Omega \qquad (3)$$

where $G(\Omega,E_p)$ = the Gibbs distribution function = $\exp(-U(\Omega,E_p)/kT)$, U = the total electrostatic potential energy = $U_1 + U_2$, U_1 = the chromophore poling field interaction = $-\mu F - (^1/_2)\alpha FF$. E_p is the applied electric poling field and F (= $f(0)E_p$) is the effective electric poling field felt by the chromophores. U_2 = chromophore−chromophore electrostatic interactions = dipole−dipole interaction + induced dipole interaction + dispersion interaction. In the approximation of London,[14] the chromophore−chromophore electrostatic interaction becomes $U_2 = W = (1/R^6)\{(2\mu^6/3kT) + 2\mu^6\alpha + 3I\alpha^2/4\}$ where R is the average distance between chromophores, α is the polarizability, I is the ionization potential, T is the Kelvin poling temperature, and k is the Boltzmann constant.

For $U_2 = 0$, $U = -\mu F\cos\theta = -\mu f(0)E_p\cos\theta$, the order parameter becomes

$$\langle\cos^3\theta\rangle = \mu F/5kT = \mu f(0)E_p/5kT \qquad (4)$$

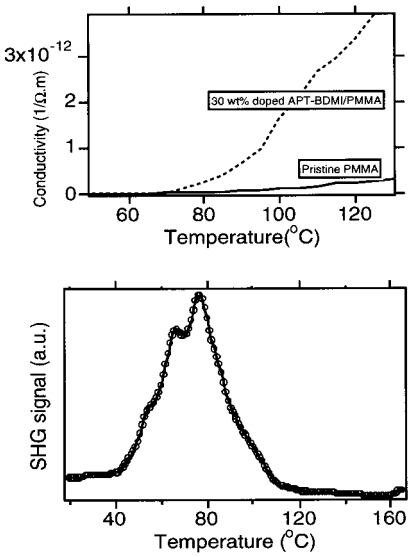

Figure 4. (Top) The variation of conductivity with temperature is shown for pure poly(methyl methacrylate), PMMA, and a solid solution of the TCI (also called APT-BDMI) chromophore (see Table 1) and PMMA. Conductivity arises from the migration of impurities as the glass-transition temperature is approached. (Bottom) The second harmonic generation (SHG) signal (which measures acentric order) is shown as a function of temperature. Note the fall off of the SHG signal due to the conductivity reducing the effective poling field.

Neglecting chromophore−chromophore interactions results in the following expression for the electro-optic coefficient r:

$$r = 2f(\omega)f(0)(N\beta\mu)E_p/5kTn^4 = 2f(\omega)f(0)(w\rho N_A)(\mu\beta/M_W)E_p/5kTn^4 \qquad (5)$$

where w = the weight fraction of the chromophore, ρ = density, N_A = Avogadro's number, and M_W = chromophore molecular weight. The critical result is that the electro-optic coefficient is predicted to be a linear function of the chromophore loading (N or w) and dipole moment. Hence, $\mu\beta/M_W$ is predicted to be a useful chromophore figure of merit (i.e., the parameter appropriate for scaling microscopic optical nonlinearity into macroscopic optical nonlinearity). Unfortunately, such simple scaling was not observed for "high $\mu\beta$" chromophores.

A number of factors can, in principle, lead to attenuation of expected electro-optic coefficients. As shown in Figure 4, electrical conductivity arising from impurities can lead to attenuation of the effective electrical poling field and to a reduction of poling efficiency. Such conductivity effects, however, are usually easily eliminated by the appropriate purification of chromophores and polymer materials. Photoconductivity of chromophore/polymer materials, induced by visible and UV light, can be a problem for a small number of materials but, even for such materials, the problem can be eliminated by simply poling in the dark. Since near-infrared light is typically employed in telecommunications applications and since modulators can be shielded from ultraviolet and visible light by packaging, such photoconductivity is not a problem for electro-optic modulator operation.

We have recently established that the problem of achieving large electro-optic coefficients for high $\mu\beta$ chromophores incorporated into polymer matrixes is

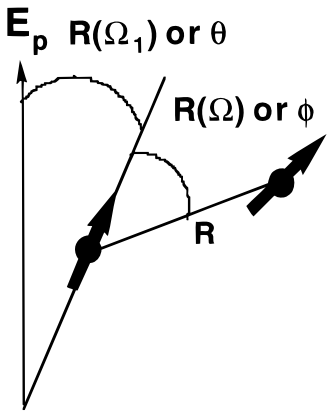

Figure 5. The spatial relationship between chromophores and the poling field and between interacting chromophores is shown. Depending on the shape of the chromophores and the anisotropy of intermolecular electrostatic interactions, either full rotation matrixes or single angles are required to relate the objects in this figure.

much more fundamental in nature and can be traced to chromophore−chromophore electrostatic interactions. In particular, if electrostatic interactions between chromophores are not neglected, then electro-optic coefficients are predicted to decrease at a high chromophore loading. The simplest (and only analytical) expression of this phenomena can be derived following the approximations of London[14] where chromophores are assumed to be spherical in shape and the interaction of one chromophore is averaged over relative orientations with respect to its neighbor. As illustrated in Figure 5, this results in the rotation matrix relating two chromophores (a general function of three Euler angles) being reduced to a single angle. Thus,

$$U = -\mu f(0) E_p \cos\theta - W\cos\phi \qquad (6)$$

$$\langle \cos^3\theta \rangle = (\mu f(0) E_p / 5kT)[1 - L^2(W/kT)] \qquad (7)$$

where L is the Langevin function. The order parameter of eq 4 is now modified to include an attenuation term $-L^2(W/kT)$ which depends on the ratio of chromophore−chromophore electrostatic energy, W, to thermal energy, kT. The result is that order parameters will now exhibit a dependence on chromophore loading (note that W is proportional to N^2) and parameters such as the chromophore dipole moment, polarizability, and ionization potential. Theoretical results shown in Figure 6 illustrate basic features of the phenomena, namely, a dramatic decrease in acentric order with a decreasing average separation which occurs over a narrow range of average separation distances, a predicted maximum in the plot of electro-optic coefficient versus chromophore loading, and a shift of this maximum to lower chromophore loading values with an increasing chromophore electrostatic interaction (μ, α, and I).

Obviously, the approximations of London will not, in general, be appropriate for real chromophores characterized, for example, by pronounced prolate ellipsoidal shapes (see Figure 7).[15,16] For such chromophores, full rotational matrixes must be evaluated leading to complex three-dimensional minimum energy/preferred orientation surfaces.[15,16] Analysis for this more complicated treatment must be carried out by numerical methods. Another appropriate modification of the theoretical model is to introduce molecular dynamics. Such treatments lead to the quantitative simulation of experimental results using experimentally determined values of μ, α, ϵ, and I as is shown in Figures 8 and 9. The effect of nuclear repulsive interactions can be carried out either in the hard object (molecules treated as spheres or ellipsoids) approximation or employing an R^{-12} repulsive potential. The comparison of experimental data for the FTC chromophore (see Tables 1 and 2) with

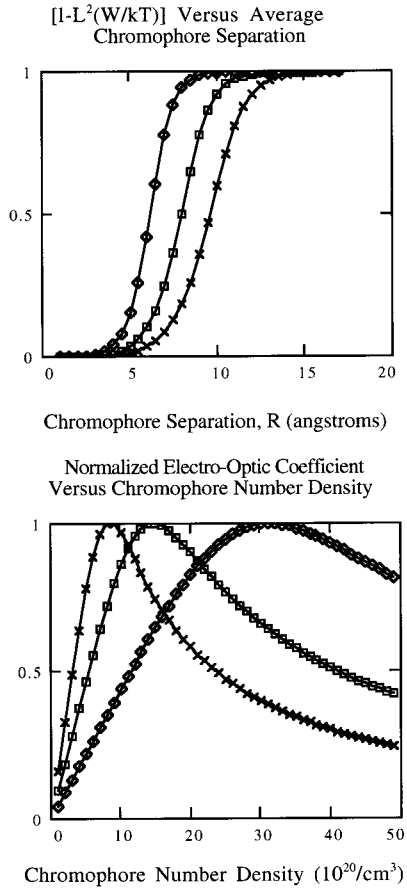

Figure 6. (Top) The variation of the attenuation of poling-induced order with average chromophore separation, R, is shown. The curves were computed assuming spherically shaped chromophores. The molecular polarizability was taken to be 3.8×10^{-23} cm^3 and the ionization potential was taken to be 8.3×10^{-19} J. Different curves correspond to variance of the chromophore dipole moment (7.5 D, solid line with squares; 5 D, solid line with diamonds; 10 D, solid line with ×'s). (Bottom) Variation of a normalized electro-optic coefficient with the chromophore number density is shown. Symbols have the same meaning as those in the upper part of the figure.

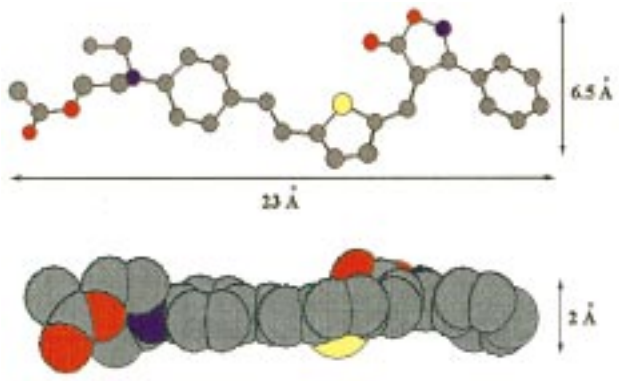

Figure 7. The crude shape of the ISX chromophore of Table 1 is shown illustrating the approximate prolate ellipsoidal shape of the molecule.

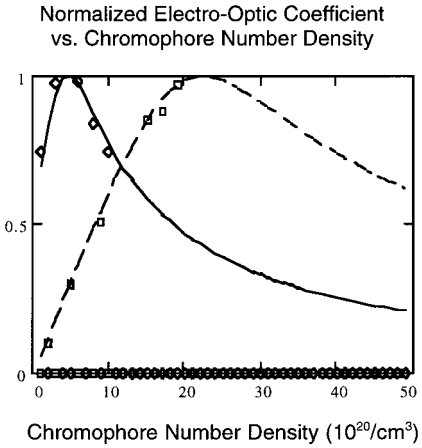

Figure 8. Theoretical (lines) and experimental (symbols) normalized electro-optic coefficient data as a function of chromophore number density, N, are compared for the DR (squares and dashed line) and ISX (diamonds and solid line) chromophores of Table 1.

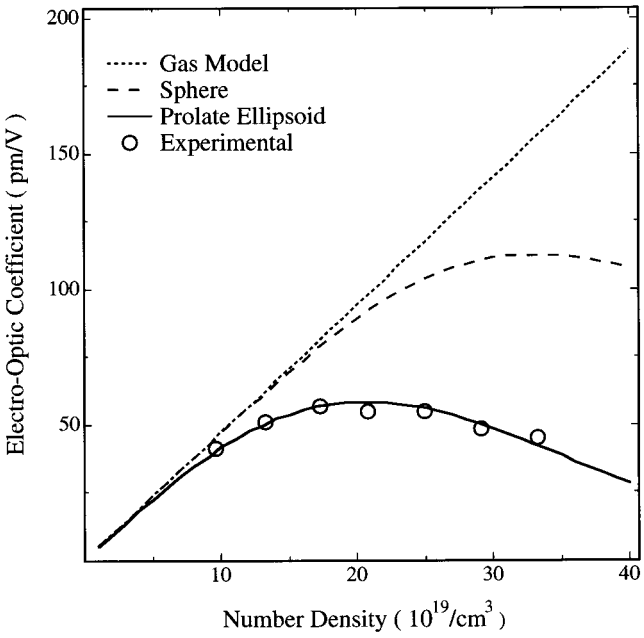

Figure 9. Theoretical (lines) and experimental (circles) electro-optic coefficients as a function of the chromophore number density are compared for the FTC chromophore (Tables 1 and 2). The solid line (which yields the best simulation of experimental data) was calculated for a prolate ellipsoidal chromophore shape. The dashed line was calculated for a spherical chromophore shape and the dotted line was calculated ignoring chromophore intermolecular interactions (the independent particle or "ideal gas" model).

theoretical calculations for spherical and prolate ellipsoidal shapes and neglecting intermolecular electrostatic calculations illustrates the critical problem of competing acentric and centric ordering forces. It is interesting to note that an oblate ellipsoidal shape would actually favor acentric order over centric order. Although this would be the theoretically desired chromophore shape, it is difficult to achieve such a shape because the intrinsically long prolate ellipsoidal shape of the electroactive π-electron core of the chromophore would require an unreasonably large amount of nonactive σ-electron periphery to realize an overall oblate ellipsoidal hydrodynamic shape. The best way one can probably achieve this in a practical sense is to attempt to approximate a spherically symmetrical shape. However, as seen from Figure 9, this could lead to a doubling of optical nonlinearity; and for the FTC chromophore

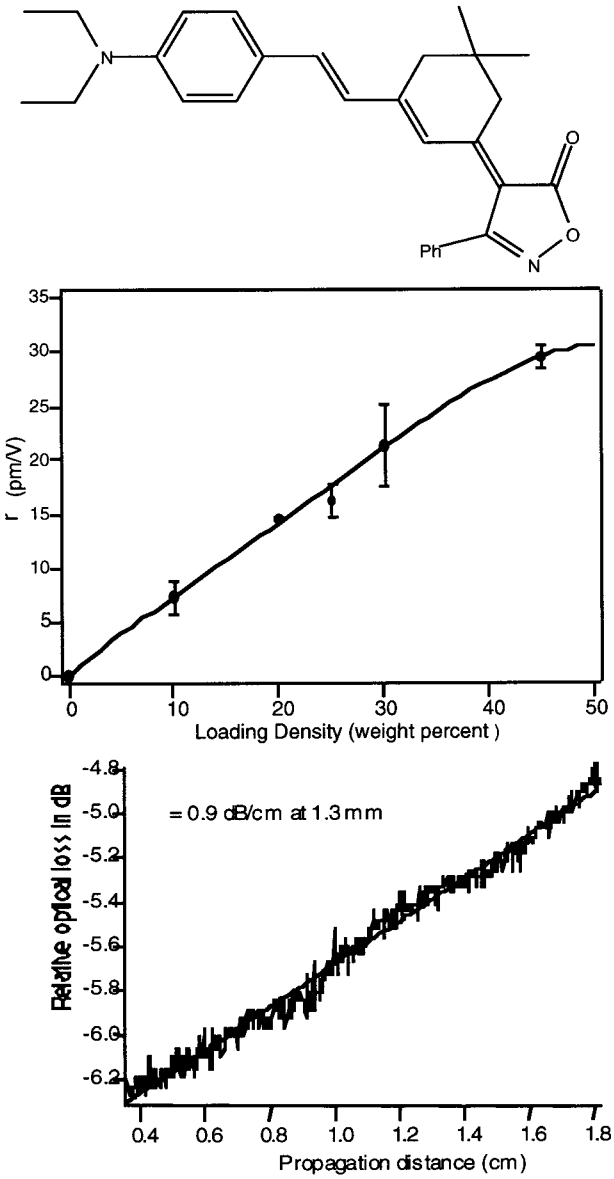

Figure 10. (Top) The structure of a high $\mu\beta$ chromophore modified to incorporate an isophorone moiety is shown. (Middle) The variation of the electro-optic coefficient for samples of this chromophore incorporated into PMMA is shown. (Bottom) The measurement of optical loss of a sample at its highest loading is shown.

of Table 2, this could mean electro-optic coefficients on the order of 100 pm/V.

On one hand, our results are depressing in that they predict that the large optical nonlinearities predicted by $\mu\beta/M_W$ scaling will never be realized. On the other hand, our theoretical results provide guidance to reduce the severity of the problem. In particular, the attenuation of macroscopic optical nonlinearity is particularly severe for prolate ellipsoidal chomophores where a close approach along the minor axes favors centric ordering.[15] Adding bulky groups to sterically inhibit such an approach is predicted to reduce the magnitude of attenuation of electro-optic coefficients observed at a high chromophore loading. We have carried out derivatization with alkyl and aryl substituents for a number of high $\mu\beta$ chromophores and have typically observed significant (factors of 2) increases in maximum achievable electro-optic coefficients.[15,16] An additional example of this effect is illustrated in Figure 10 where the isophorone group is used to inhibit the close approach

along minor axes.[17] The best fit simulation requires a shape intermediate between that of the ellipsoid best describing the unmodified chromophore and a sphere.[17] Note that the isophorone group is oriented orthogonal to the isoxazalone acceptor group, thus providing maximum steric inhibition to a close approach. Note also that a 1−2 Å change in the close approach along the minor axes can have a dramatic effect the on attenuation of optical nonlinearity as suggested by Figure 6 (top).

Of course, steric modifications of chromophores must be achieved without perturbation of the π-electron structure because such perturbation will change the molecular hyperpolarizability β. We have found, in some cases, derivatization causes a conformational change that can either disrupt or enhance π-orbital overlap. Fortunately, such perturbation is readily apparent from a shift in the λ_{max} of the absorption spectrum of the chromophore.

Derivatization of high $\mu\beta$ chromophores for steric inhibition of the close approach and attenuation of optical nonlinearity has permitted electro-optic coefficients in practical device materials to be increased from values of 5−15 pm/V to values of 30−80 pm/V (at 1.3 μm),[17−20] finally becoming competitive with lithium niobate.

Before concluding our discussion of the optimization of electro-optic coefficients, it is useful to mention techniques used for the experimental definition of electro-optic coefficients. Measurement techniques include ellipsometry,[21,22] attenuated total reflection (ATR),[23] and two-slit interference modulation.[24,25] Second harmonic generation is also an effective tool for in situ monitoring of poling efficiency and retention of poling-induced second-order optical nonlinearity.[26] Recently, we have introduced a modified version of the ATR technique amenable to the measurement of a larger number of samples in a short period of time.[27,28]

Another interesting point concerning derivatized high $\mu\beta$ chromophores is that materials fabricated using these chromophores frequently exhibit lower optical loss than materials fabricated using underivatized chromophores. In the example shown in Figure 10, an optical loss of approximately 0.9 dB/cm (at 1.3 μm) is observed for the chromophore-containing polymer while values of greater than 1.0 dB/cm (at 1.3 μm) are observed for underivatized chromophores.[17] Similar observations have been made by Wang[20] for a number of chromophores. This aspect of optical loss, which derives from light scattering off chromophore aggregates, can also be understood from a consideration of the theory of chromophore−chromophore electrostatic interactions. Two regions of behavior are predicted as a function of the relative magnitudes of chromophore−chromophore electrostatic interaction energies and thermal energies. When the values are comparable, the effect of chromophore−chromophore interactions can be considered a local field effect ("transient aggregation"). The chromophores can be considered to be ordered by an effective field determined by the vectorial combination of the chromophore−electric field and chromophore−chromophore interaction fields. Aggregates of sizes appropriate for light scattering are not predicted to exist. However, when chromophore−chromophore electrostatic interaction energies significantly exceed thermal energies, nontransient aggregation results. This is particularly a problem for prolate ellipsoidal chromophores. When aggregate sizes begin to approach the wavelength of light, light scattering (optical loss) increases dramatically. A signature of this effect is a dramatic, nonlinear increase in optical loss versus chromophore loading.[28] Optical loss can dramatically increase from approximately 1 dB/cm (at 1.3 μm) to greater than 10 dB/cm (at 1.3 μm) over a narrow range of chromophore concentrations. To illustrate this point, consider the following optical loss (at 1.3 μm) data from the thesis of A. Chen:[28] A 5 wt % solid solution of the disperse red (DR) 19 chromophore (see Table 1) in poly(methyl methacrylate), PMMA, exhibits an optical loss of 1.03 dB/cm, while 5 wt % of the tetracyanoindane (TCI) acceptor chromophore (see Table 1) in PMMA yields an optical loss of 8.7 dB/cm, and 5 wt % of the Sandoz (SDS) chromophore (see Table 1) in PMMA yields an optical loss of 19.3 dB/cm. This trend qualitatively reflects the trend in chromophore electrostatic interactions for this series of chromophores. Optical loss has also been investigated as a function of the chromophore number density for a number of chromophores.[28] At low-to-modest chromophore concentrations (for either chromophore/polymer solid solutions or for chromophores covalently attached to polymers), optical loss is observed either to be constant or to increase in a linear manner with chromophore loading (depending on the measurement wavelength). However, at some higher loadings (after the onset of attenuation of macroscopic second-order optical nonlinearity) optical loss is observed to increase in a highly nonlinear manner with chromophore concentration.

Optical loss was typically measured by the method of immersion in a high index fluid.[29]

Nontransient aggregation can also inhibit lattice hardening reactions to be discussed in the next section. Again, as with electro-optic attenuation and optical loss issues, such effects can be minimized by appropriate chromophore modification.

4. Stabilization of Acentric Order

To be useful for the fabrication of prototype electro-optic modulator devices, acentric chromophore order induced by electric field poling must be stable for long periods of time at temperatures encountered in device operation and for shorter periods of time at the even higher temperatures encountered in device fabrication. In practice, we have found that this requires a material that exhibits greater than 95% retention of optical nonlinearity for 1000 h at 100 °C.

To achieve such thermal stability, the chromophores must be coupled effectively to a high glass transition, T_g, polymer lattice. Although some research groups still advocate the use of chromophore/polymer composites (or solid solutions) fabricated using high T_g polymers such as polyimides, thermally stable materials have more frequently been prepared exploiting covalent coupling of chromophores to a polymer matrix.[1] For best results, both ends of the chromophore are coupled to the polymer matrix as shown in Figure 11.

Two general approaches have evolved for the production of hardened acentric lattices. The first can be considered a prepolymer (or two-step) route shown in Figure 11 while the second can be considered to be a single-step thermosetting scheme such as that shown in Figure 12. In both schemes, the final hardening reaction is a thermosetting (condensation) reaction. In the first approach, the prepolymer can be formed employing a variety (condensation, free radical, ring-

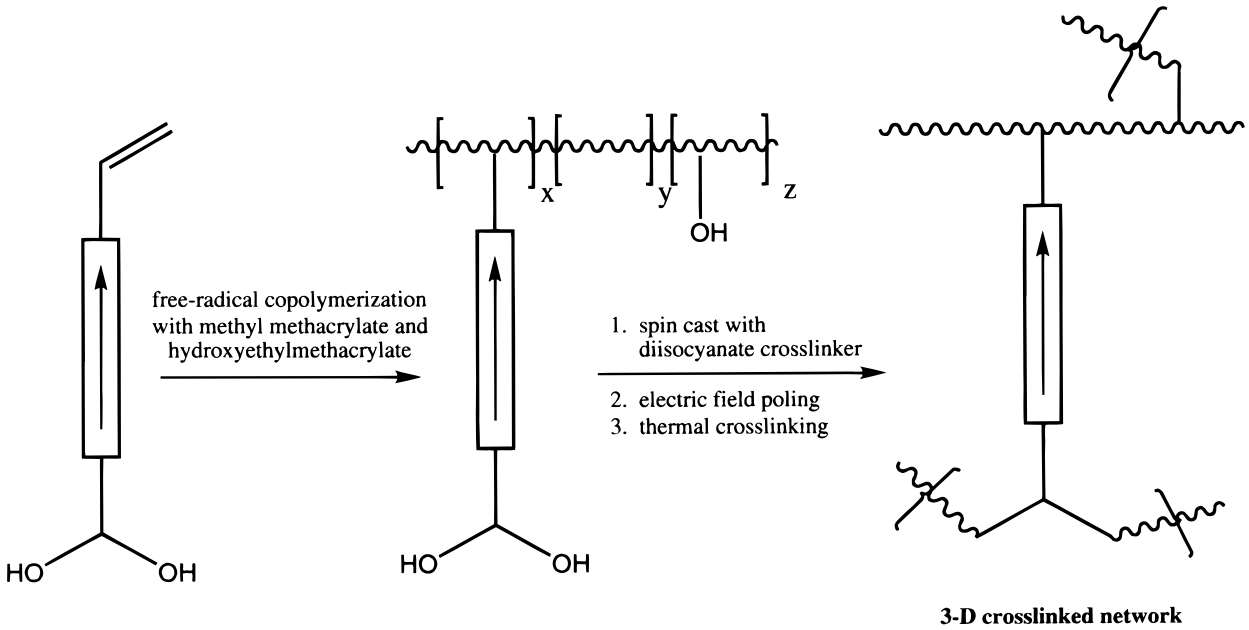

Figure 11. A two-step (polymer precursor) lattice hardening protocol is illustrated.

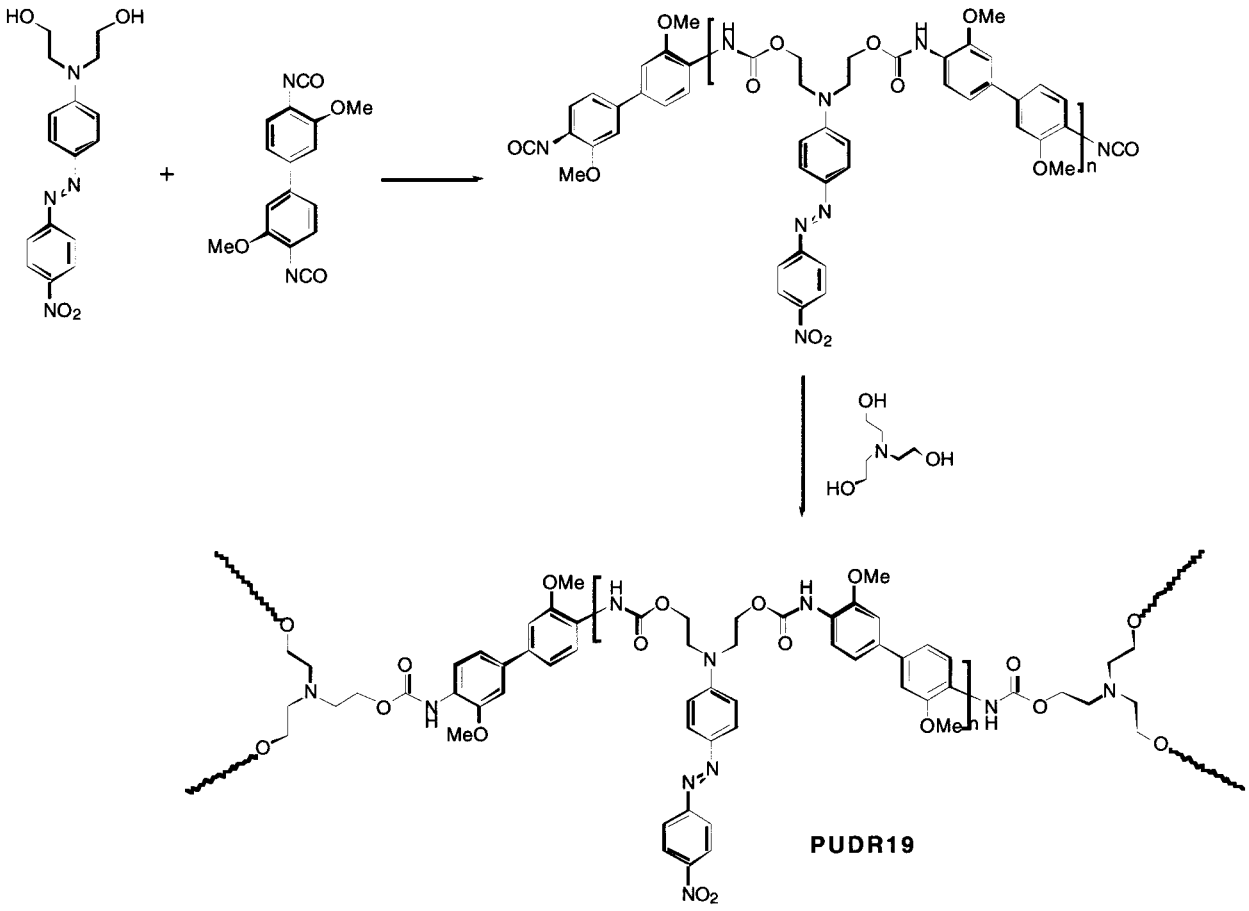

Figure 12. The thermosetting reaction producing the PU-DR19 material discussed in the text is shown. Note that only one end of the chromophore is covalently coupled to the polymer lattice.

opening metathesis polymerization (ROMP)) of polymerization reactions. The prepolymer approach has the additional advantage of permitting a degree of separation of the poling and lattice hardening steps. The second scheme, where these two processes always occur to some extent simultaneously, has been widely used in the fabrication of prototype devices because of to the ease of preparing large quantities of materials and because high chromophore loading is easily achieved.

An approach which has recently gained some popularity is to utilize both intramolecular and intermolecular condensation reactions to (1) stiffen the main-chain polymer backbone and (2) couple the chromophore at both ends to the polymer main chains with the chro-

mophore acting as a cross-linking moiety.[30,31] Ideally, the intramolecular condensation occurs as the final step and acts simply to increase the glass-transition temperature of the final polymer lattice. Essentially, the final matrix consists of a chromophore attached at both ends to a polyimide-like (heteroaromatic) cross-linked polymer matrix.[30,31] The concept is to arrive at the final matrix in a series of steps which permits good solubility and a low glass transition through spin casting and poling stages but yields an exceptionally thermally robust final electro-optic material.

A common problem to all approaches which involves more than one component is that of phase separation. With thermosetting schemes this can be particularly problematic since a number of oligomeric structures are formed as intermediates to the final hardened material.[32] Moreover, with thermosetting schemes, the hardening process is occurring during all processing stages (spin-casting, poling, and lattice hardening to stabilize poling-induced order). Indeed, an initial hardening (precuring) step is typically used to increase viscosity to an appropriate level for spin casting optical quality thin (1−2 μm) films. The films are then heated to a temperature near the glass-transition temperature and poled. Because the glass-transition temperature is increasing with time as the lattice hardening condensation reactions proceed, poling is typically carried out in a series of temperature steps for best results. Because hardened materials are able to withstand greater voltages without damage, applied voltage is also typically increased in a stepwise fashion. Immediately after each temperature step, the lattice softens, permitting the chromophores to reorient under the influence of the poling field. As the lattice hardening proceeds driven by the elevated temperature, the lattice becomes too hard to permit further chromophore movement and another temperature step is required. Because the acentric order $\langle\cos^3\theta\rangle$ which is finally achieved and the thermal stability of the hardened lattice are determined by the kinetics of the hardening reactions and chromophore molecular dynamics in various lattice structures, exact results will depend strongly upon the precise processing protocols used.

In carrying out lattice hardening, it is important not only to increase the thermal stability of poling-induced second-order optical nonlinearity but also to do so without increasing optical loss. In discussing the effectiveness of various hardening protocols, it is necessary to quantify both the thermal stability and optical loss; thus, let us turn our attention to the measurement of these variables. Of course, thermal stability can be measured by simply maintaining the material at a fixed temperature and measuring second-order optical nonlinearity (electro-optic coefficient or second harmonic generation coefficient) as a function of time. However, this method is time-consuming and not particularly useful for comparing materials. A more useful measurement of the thermal stability of optical nonlinearity is achieved by ramping the sample temperature (e.g., at a rate of 5 °C/min) while monitoring second-order optical nonlinearity (e.g., second harmonic generation).[26] In Figure 13, we compare data for the thermosetting material of Figure 12 and for the thermosetting material of Figure 14 using this dynamic assay of the thermal stability of optical nonlinearity. The data shown in Figure 13 illustrate the point made earlier that attaching both ends of a chromophore to a cross-linked polymer lattice invariably results in improved thermal stability of the poling-induced optical nonlinearity relative to that obtained for single-end attachment.

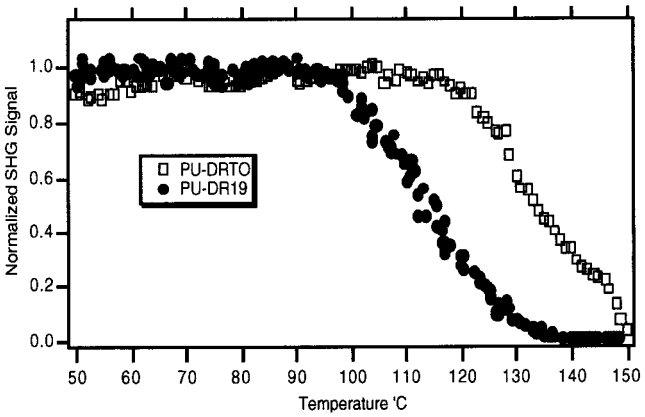

Figure 13. The variation of second-order optical nonlinearity (monitored by second harmonic generation) is shown for the PU-DR10 material of Figure 12 and the PuDRTO material of Figure 14. Note the improved thermal stability of poling-induced acentric order when both ends of the chromophore are covalently coupled to the polymer lattice.

Optical loss is measured by immersing the nonlinear optical material into a high index liquid which results in the out-coupling of light from the material. Thus, the distance of light propagating through the material can be systematically varied by varying the extent of immersion into the high index fluid, permitting the measurement of the out coupled light intensity (or conversely optical loss) versus propagation distance in the material. This technique has the advantage of being nondestructive and permitting insight into material inhomogeneity. We also measure optical loss by other methods such as the cutoff method but the above-mentioned immersion method, which is illustrated in Figure 15 (measuring optical loss of samples with different precuring times), is the most useful.

The data in Figure 15 provide a useful introduction into the concept of poling-induced optical loss. Poling-induced optical loss has been a poorly understood phenomena and many researchers have assumed that it is always large and unavoidable for organic materials. In reality, poling-induced optical loss arises either from surface damage during poling or from migration of chromophores under the influence of the poling field. In some cases, surface damage can be quantitatively investigated by surface characterization techniques such as secondary ion mass spectroscopy (SIMS). Such investigations indicate that optical loss due to surface damage is less severe the harder the polymer lattice. We have found that, by careful control of processing conditions, poling-induced optical loss can be reduced from ≈9 to 0.2 dB/cm.[32] Optical loss due to chromophore migration also depends on lattice hardness. The problem is most severe for chromophore/polymer composite materials and becomes less problematic the more tightly the chromophore is coupled to the polymer lattice. Thus, like surface damage effects, processing to yield harder lattices at critical poling stages reduces optical loss because of migration. The previously quoted reduction reflects the decrease of both types of poling-induced losses. A number of workers have dealt with the problem of poling-induced optical losses and we do not attempt a comprehensive review of that literature here. For further references on this subject the reader is referred

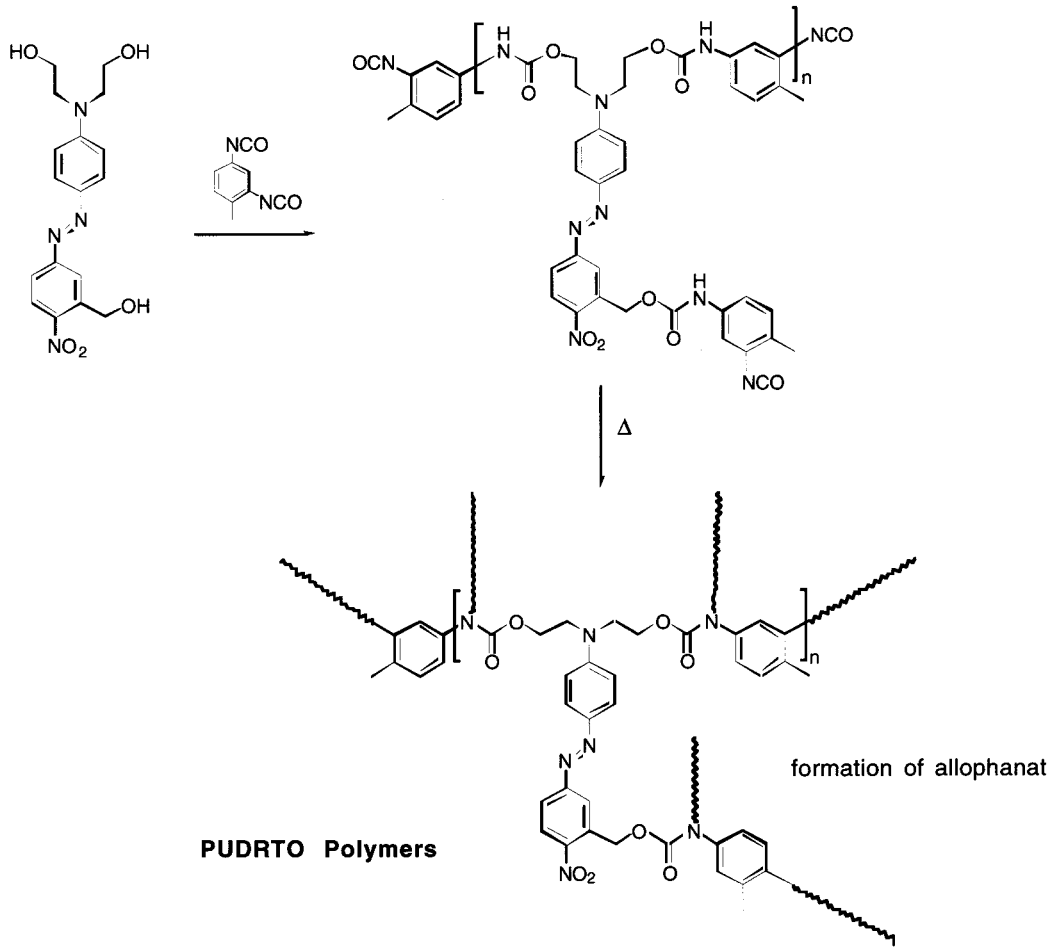

Figure 14. The thermosetting reaction producing the PUDRTO material discussed in the text is shown.

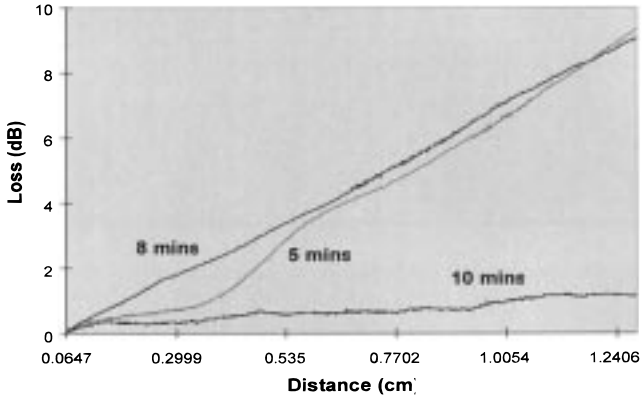

Figure 15. Measurement of optical loss (dB/cm) as a function of precuring time for a thermosetting polymer is shown.

elsewhere.[33−35] The reader is particularly referred to the attempted quantitative theoretical treatment of poling-induced optical loss by Teng and co-workers[33] which provides useful insight into loss mechanisms.

Figure 15 illustrates the importance of the precuring time. Not only does the precuring time define viscosity, which is relevant to spin-casting optical quality films, but it also defines optical loss and poling efficiency (through control of chromophore mobility). Obviously, there is a tradeoff between too much hardening which leads to poor poling efficiencies (small electro-optic coefficients) and poor quality films due to inappropriate spin-casting conditions and too little hardening which leads to high optical loss and poor thermal stability of poling-induced electro-optic activity.

Like precuring, poling itself must be carried out in a manner which leads to acceptable values of the electro-optic coefficient, thermal stability of the poling-induced optical nonlinearity, and optical loss. For thermosetting materials, a stepped protocol, where both the temperature and electric field are increased in time, typically works best as is to be expected from the above remarks.

Three-dimensional polyurethane polymer lattices, such as those shown in Figures 12 and 14, have been particularly popular electro-optic materials because of the ease of synthesis, the ability to form good optical quality films, their high glass-transition temperatures, and solvent resistance (which is important for the deposition of cladding layers). The properties of polyurethanes are well-known to be strongly affected by the composition and stoichiometry of OH and NCO functionalities. For example, polymers, such as the PUDRTO polymer of Figure 14, which contains excess isocyanate groups can self-react to form allophanate linkages. Neutralization of these excess isocyanate groups with triethanolamine (TEA) yields *n*-PUDRTO-type materials (Figure 16). It is clear from consideration of the structures shown in Figures 14 and 16 that these two materials should yield different properties and they do as is evident from a consideration of the experimental data presented in Table 5. In particular, it is readily apparent from Table 3 that adjusting the NCO/OH ratio to unity by the addition of TEA results in materials with acceptable levels of optical loss, electro-optic coefficients, and thermal stability. Without such treatment, cloudy films are obtained presumably from reaction of NCO

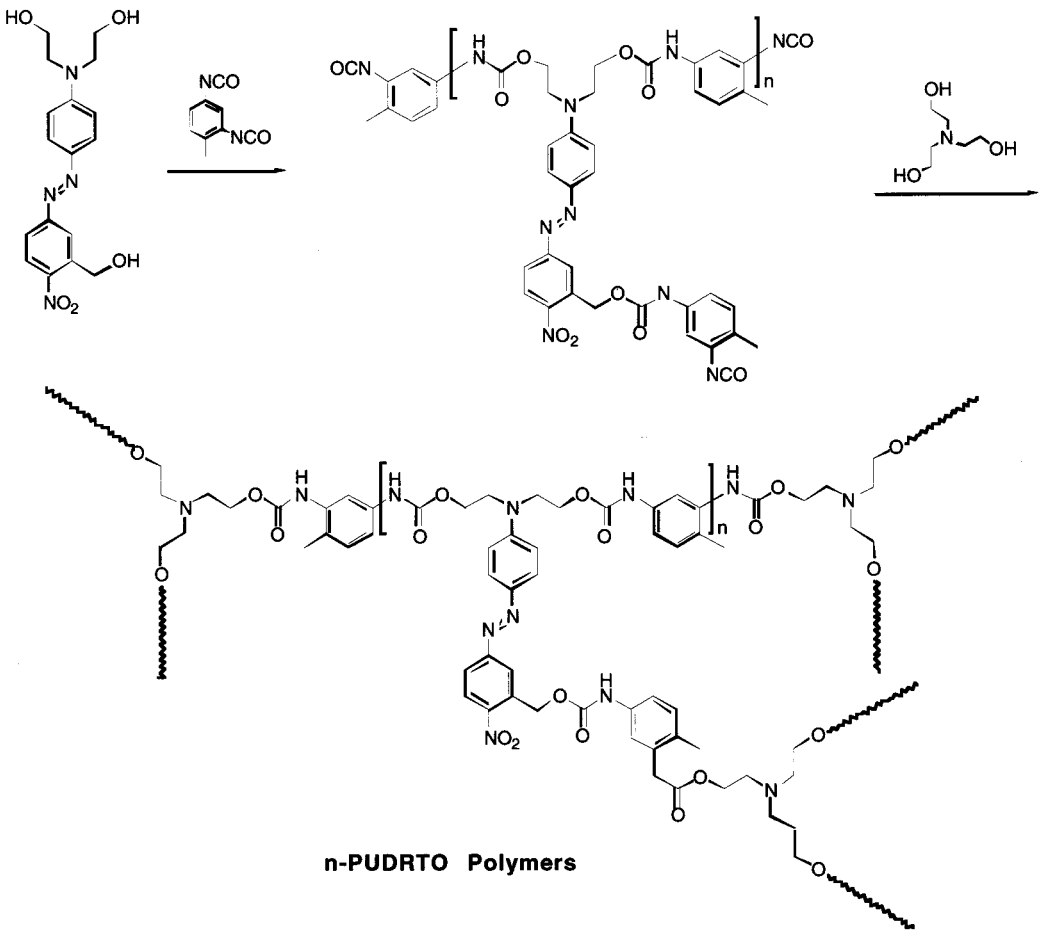

Figure 16. The preparation of *n*-PUDRTO polymer materials is shown.

Table 5. Linear and Nonlinear Optical Properties of PUDRTO Polymers

polymers	LD (%)[a]	NCO/OH	M_w/M_n[b]	n[d]	r_{33} (pm/V)[c]	T_{stab} (°C)[f]	loss (dB/cm)
PUDRTO−1	42	1.6	800/590	1.720	10	120	N/A
PUDRTO−2	35	2.2	590/430	1.640−1.720	14.4	110−120	6.6
n−PUDRTO−1	37	1.0	980/640[c]	1.689−1.692	14.8	110	0.86
n−PUDRTO−3	32	1.0	1200/700[c]	1.675−1.676	12	115	1.0

groups with atmospheric water or from aggregation of excess tolylenediisocyanate (TDI) molecules.

The oligomeric nature of various PUDRTO and *n*-PUDRTO materials during the precuring stage is evident from the gel permeation chromatography (GPC) data shown in Figure 17. The data shown here also suggest that the TEA−TDI molecules aggregate and contribute to optical loss in the *n*-PUDRTO materials as do the TDI molecules in PUDRTO materials.

Similar control of conditions are required for other thermosetting approaches including sol−gel processing.[1,36,37] The two-step (or precursor polymer) approach, based on asymmetrically functionalized chromophores (chromophores whose end functionalities exhibit different reactivities for coupling to the polymer matrix), avoids problems associated with low-molecular-weight oligomers but still requires consideration of phase separation involving prepolymer and cross-linking reagents.[1,38] It is more difficult to achieve high chromophore loading with this approach; nevertheless, this approach yields materials comparable to the best materials obtained by thermosetting approaches. Both approaches have yielded thermally stable materials used in the fabrication of prototype devices (to be discussed in the following sections).

Unfortunately, lattice hardening has largely been achieved by using thermosetting reactions involving the condensation and elimination of water. These reactions tend to be sensitive to atmospheric moisture and storage of cross-linking reagents can be a problem. A substantial effort has been made to find photo-cross-linking reactions which could be utilized to achieve lattice hardening.[1] Unfortunately, reactions explored to the present time suffer from the interference of nonlinear optical chromophore absorption with that of the photoactive cross-linking functionality. An alternative, which has yet to be explored, is the use of two-photon cross-linking moieties.

Again, we have not attempted a comprehensive review of lattice hardening in a poled polymer system. For more insight into the extensive literature on this subject the reader is referred elsewhere.[1,39]

5. Fabrication of Low-Loss Buried Channel Waveguides

A critical step in the fabrication of all electro-optic devices from nonlinear optical materials is the processing of materials into buried channel waveguides surrounded by material with a lower refractive index.

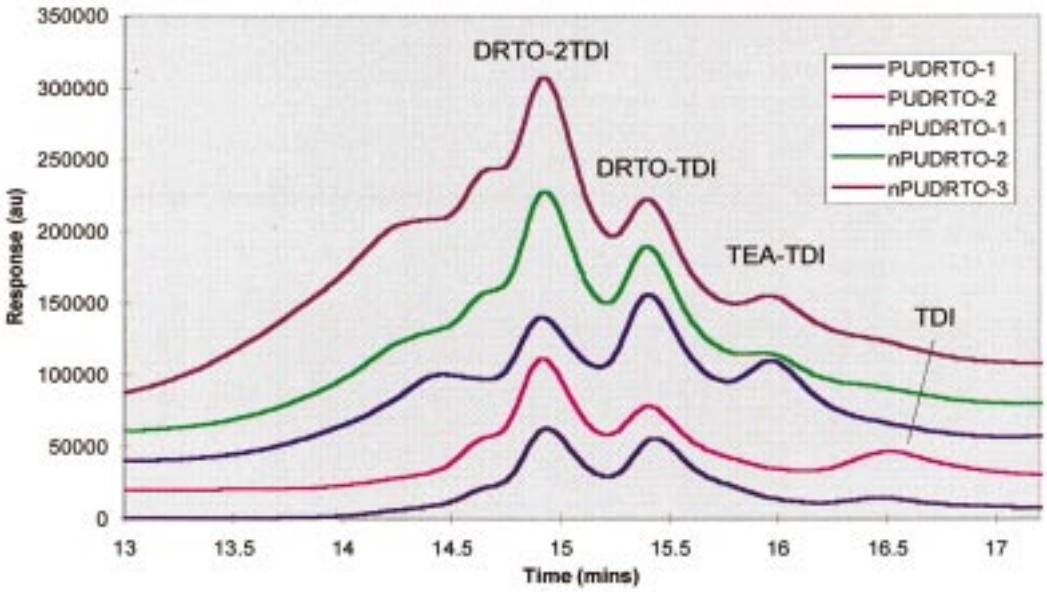

Figure 17. GPC traces of PUDRTO prepolymers before electric field poling. From bottom to top (see Table 5): PUDRTO-1, PUDRTO-2, *n*-PUDRTO-1, *n*-PUDRTO-2, and *n*-PUDRTO-3.

Polymeric buried channel waveguides have most commonly been fabricated employing either photolithography or reactive ion-etching techniques. We have developed a photochemical processing technique, which we refer to as multiccolor photolithography, which permits the processing of buried channel waveguides without the deposition of cladding layers and which permits straightforward fabrication of tapered transitions between waveguides of different dimensions. Multicolor photolithography (MCP)[1] is based on the principal that light of different wavelengths (for wavelengths near a photoactive chromophore absorption) will exhibit different penetration profiles into a sample reflecting the wavelength-dependent absorption coefficient of the photochromic transition. An excitation of a photochromic transition produces a conformation change of the chromophore, which, in turn, produces a change in absorption and index of refraction of the material. The precise change in the index of refraction is determined by the photochemical kinetics and thus by light intensity and time of exposure. Since chromophore absorption (wavelength of light) can be used to produce a precisely defined light intensity variation in a sample, virtually any desired spatial variation of the index of refraction can be achieved by control of the wavelength and exposure time of radiation exciting a photochemical transition.

Fabrication of a buried channel waveguide without the deposition of a cladding layer is accomplished in the following manner: A thin film of nonlinear optical material containing a photochromic dye is spun onto a substrate with a lower index of refraction. With the desired waveguide area (high-index region) of the nonlinear optical film protected by a mask, the sample is irradiated for a "long" period of time with light of a wavelength corresponding to the tail of the photochemical transition of the dye. Such light is not attenuated by absorption, so it penetrates uniformly through the sample. Since this light produces photochromic conformation change only very slowly, a "long" exposure time is needed to create uniform low index of refraction regions on either side of the protected high-index nonlinear optical material region (channel). In a second exposure step, the sample is exposed for a "short" period of time to light of a wavelength near the maximum of the photochromic transition. Because of high absorption, such light exhibits shallow penetration and bleaches only the uppermost region of the high-index nonlinear optical material (providing the exposure is short). The end result of the two exposure steps is a high index of refraction nonlinear optical material core (waveguide) surrounded by lower index material. On the bottom, the low index of refraction is provided by the substrate. On the two sides and on top of the active waveguide, low-index regions have been generated by photochemical reactions, the extent of which has been controlled by the control of wavelength and exposure time. By introducing scanning (spatial translation of the monochromatic radiation), tapered transitions can be effected.

Although MCP (and scanning MCP) can produce low-loss waveguides (and tapered transitions) and is a totally dry process, multicolor photolithography requires a photochromic material.[40] The most commonly used chromophore has been the disperse red chromophore which also provides second-order nonlinear optical activity. The two most common concerns for waveguides fabricated in this manner include the degradation of waveguide structures by environmental or operational light and the difficulty of incorporating photochromic dyes when nonphotochromic high $\mu\beta$ chromophores are employed.[40] The problem of degradation of waveguides by operational light at wavelengths of 1.3 and 1.55 μm does not appear to be as problematic as originally anticipated. These operational wavelengths are far removed from the maximum of photochromic transitions (which is typically less than 500 nm), and so the transition matrix (photochemical rate) at the operational wavelength is extremely small even for intense optical fields. Of course, care must be exercised in ensuring that multiphoton processes do not contribute to photochemically induced conformational (index of refraction) changes. Visible light, which can directly and efficiently excite photochemical change, can be excluded by encapsulating the material. The more serious problem is modifying nonphotochromic materials so that they are suitable for photolithographic processing. While

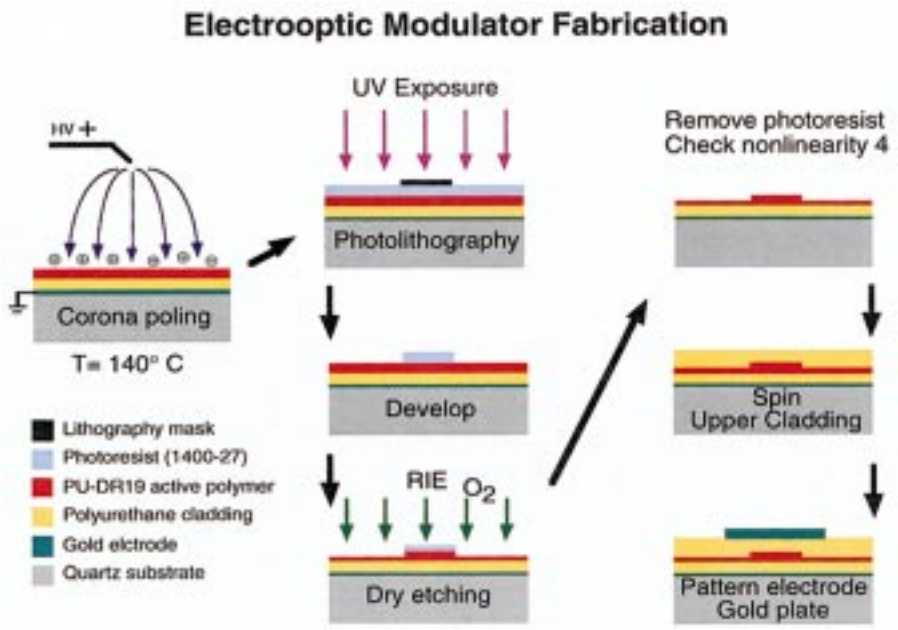

Figure 18. The steps involved in electro-optic modulator fabrication employing reactive ion etching are shown.

in principle this can be accomplished, it has not been pursued to this point in time. Thus, we shall restrict our further remarks to reactive ion-etching techniques since such techniques are applicable to any polymeric nonlinear optical material and are, initially at least, the techniques preferred for fabricating buried channel nonlinear optical waveguides in a high $\mu\beta$ chromophore containing polymer thin films. Although polymeric waveguides have been fabricated by laser ablation techniques,[41,42] we refer the reader elsewhere for a review of these and other waveguide fabrication methods other than RIE.[1]

The procedure for fabricating buried channel waveguides by reactive ion etching (RIE) is shown in Figure 18 (illustrated in detail for a disperse red 19 chromophore containing polyurethane polymer, PU-DR19). The critical question to be answered is whether waveguides of acceptably low optical loss can be fabricated by the control of the conditions of reactive ion etching. As can be seen from the data shown in Figure 19, the answer is an unequivocal "yes". By reducing the kinetic energy of the reactive oxygen ions, waveguide loss due to wall roughness (confirmed by electron microscopy[20]) can be reduced to 0.01 dB/cm which is insignificant.[20,43,44] Such low kinetic energy ions correspond to the conditions of a "chemical" etch and waveguide surface roughness can be traced to pitting because of the collision of ions with high kinetic energy with the surface. The RIE conditions which lead to lowest optical loss will vary from material to material. Electron cyclotron resonance (ECR) etching has also been investigated by Steier and co-workers. This technique provides even better control over the reactive plasma and typically leads to superior results relative to RIE. Hyperthermal atom etching has also been investigated and offers certain advantages; however, it is clear that RIE is a completely adequate protocol for polymeric buried channel active waveguide fabrication, providing optimum etching conditions are defined.

If optical loss for an optical wave propagating through a polymeric electro-optic modulator waveguide is to be kept to reasonable values, the optical wave must not "see" the lossy metal drive electrodes. Thus, cladding layers must shield the optical wave from the electrodes. Several critical considerations must be kept in mind when fabricating cladding layers. High-cladding conductivity can result in low V_π voltage at low frequencies because the modulation voltage drop across the cladding is smaller. However, as the frequency becomes higher, the conductivity has a weaker influence on the voltage distribution than the dielectric constants in each layer and the V_π increases sharply with the frequency. Thus, core and cladding conductivities and dielectric constants must be considered in light of particular applications. Core and cladding materials must be "compatible" in two ways: (1) Their intermolecular interactions should lead to a strong interface so that delamination is not a problem and (2) solvents required for the deposition of cladding layers should not attack the electroactive polymer layer. A great deal of attention has been given to cladding material choice and processing by researchers at Lockheed/Martin, USC, and elsewhere, but very little of the research has been published. This area of polymeric electro-optic device fabrication remains in the category of "art" which makes it no less important than other topics but more difficult to review here.

6. Coupling a Polymer Waveguide to Silica Fibers

Obviously, light has to be coupled in to and out of polymeric electro-optic modulator waveguides. For simple prototype device demonstrations, researchers have employed prism or crude butt coupling. Clearly, for practical (commercial) applications, such coupling schemes are inappropriate and attention must be given to the integration of the polymeric modulator waveguide with silica optical transmission fibers and with diode laser sources. The problems encountered in silica fiber and diode laser coupling are similar; for the sake of brevity, we will focus only on the former here.

There are two aspects to the integration of polymeric waveguides with silica fibers: The first is the realization of mechanically stable and precisely aligned coupling and the second is the minimization of optical loss due to mode size mismatch in the two types of waveguides.

REDUCTION IN WAVEGUIDE LOSS BY SYSTEMATIC REACTIVE ION ETCHING

Optical loss at 1.3 mm wavelength due to waveguide surface roughness as a function of the conditions of reactive ion etching

(Proc. SPIE, 413, 147-58, 1996)

Oxygen Flow Rate sccm	Oxygen Pressure mT	Rf power Watts	Optical Loss dB/cm
25	50	95	0.93
25	175	100	0.74
25	175	60	0.41
25	400	15	0.05
50	400	12	0.01

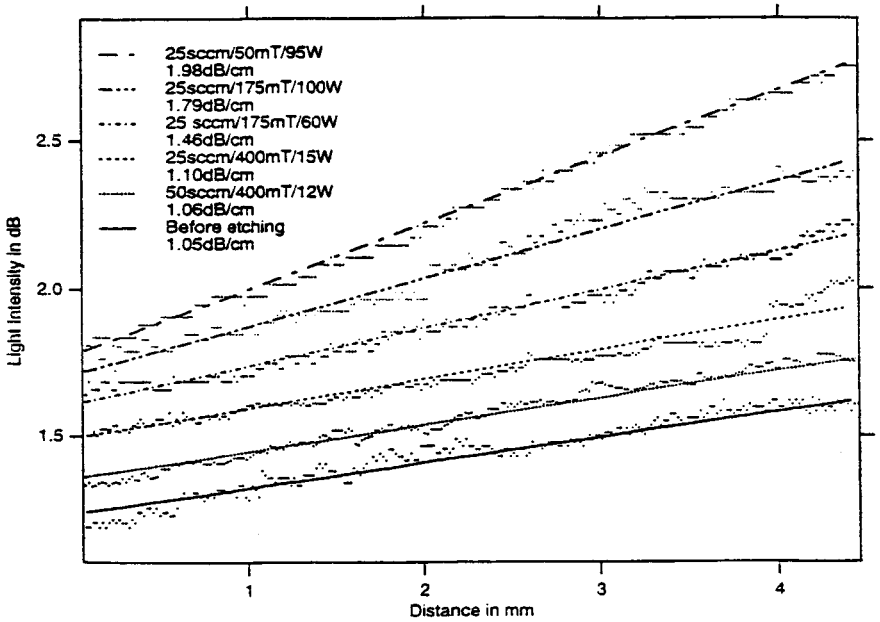

Figure 19. The variation of waveguide loss due to wall surface roughness is shown as a function of RIE processing conditions.

Note that because of quite different performance requirements, the polymeric modulator and silica fiber transmission waveguides have quite different dimensions at an operational wavelength of 1.3 μm. Efficient electro-optic modulation requires single optical mode transmission and the requirement of low drive voltage necessitates small electrode spacings and hence small waveguide vertical dimensions. A typical active polymeric waveguide has a lateral width of 5 μm and a vertical dimension of 1−2 μm. Thus, the supported mode is elliptical in shape and defined by these dimensions. However, a silica fiber designed for the long distance transport of a 1.3 μm light has a core diameter of approximately 10 μm and supports a comparable spherical optical mode.[45] The size difference in modes in these two waveguides can lead to coupling losses of 4−6 dB/connection. Since the total optical loss is determined by the combination of transmission and coupling losses and since transmission losses are small (approximately 1 dB/cm if processing is appropriately controlled—see previous sections) compared to coupling losses, it is critically important for telecommunication applications to reduce coupling losses. We shall shortly demonstrate that, by the utilization of vertically tapered mode size transformers, coupling losses can be reduced to less than 2 dB/connection. However, first let us review the achievement of mechanically stable coupling of silica fibers to polymeric waveguides.

Silicon v-groove technology, where anisotropic chemical etching[46,47] is used to etch a v-shape groove in a silicon substrate, affords a convenient and efficient means of reproducibly positioning silica fibers[48,49] relative to polymeric waveguides and provides a platform for the development of mechanically stable coupling by polymer overcoating of silica fibers placed in silica v-grooves. The process is illustrated in Figure 20. Anisotropic wet chemical etching of ⟨100⟩ oriented silicon by potassium hydroxide results in 100 times faster etching in the ⟨110⟩ direction than in the ⟨111⟩ direction leading to v-groove development. v-Grooves and polymer waveguides are fabricated on the same substrate using matched alignment marks ensuring

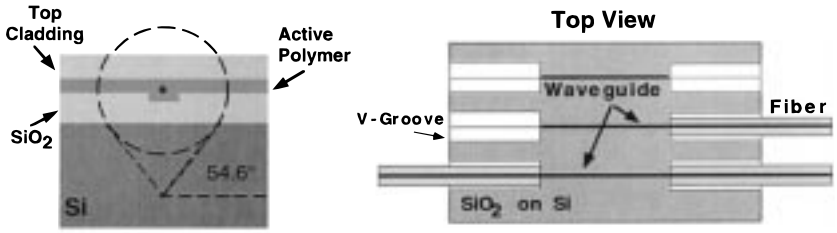

Figure 20. Schematic representations of polymer waveguide−silica fiber coupling utilizing silicon v-groove technology are shown.

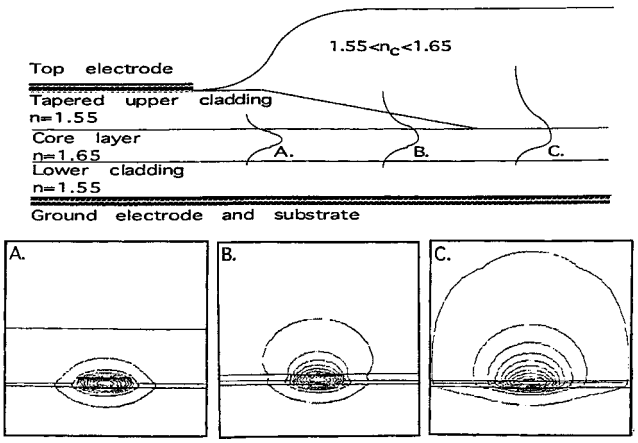

Figure 21. (Top) A schematic representation of a vertical tapered mode size transformer is shown. (Bottom) Theoretically predicted mode profiles are shown at points A, B, and C in the taper.

accurate and reproducible alignment of fibers and polymer waveguides.[48,49]

Vertically tapered mode size transformers are fabricated on already processed waveguide devices; thus, this circuit modification is independent of previous device processing steps.[20,50−53] An advantage of such mode size transformers fabricated beyond the end of electro-optic waveguide structures is that mode expansion is allowed to occur in directions where optical loss is not increased because of interaction with lossy structures such as modulator electrodes and substrates.

We have used reactive ion etching to fabricate 0.5−2 mm length tapers in the low-index upper cladding to reduce its thickness from several μm to zero, followed by the coating of a second upper cladding with an index higher than that of the previous upper cladding but slightly lower than that of the active waveguide core (see Figure 21).[20,50−53] In the taper, the buried channel waveguide mode gradually loses confinement by the upper cladding so that the mode size expands as the light propagates in the taper. In contrast, the confinement by the lower cladding and lateral confinement are hardly affected. The bottom part of Figure 21 shows theoretically predicted mode behavior (calculated using Fwave IV, a freeware for waveguide mode calculation; an adaptive vectorial finite difference method was used to calculate local modes in the taper and the results were verified with the Fourier decomposition method). Experimental behavior is demonstrated in Figure 22 and is consistent with theoretical predictions. Theory indicates that the lowest coupling loss that can be achieved is limited by the asymmetric nature of the expanded mode in the vertical direction. Theory suggests that for the vertical mode transformer described, the minimum loss is approximately 1 dB. Coupling loss due to a lateral mismatch of polymer and silica fiber modes is less than 0.1 dB.

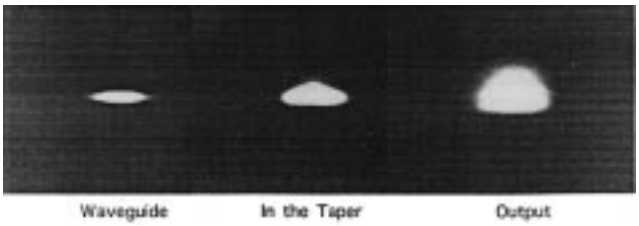

Figure 22. Photographs of the expanded modes in experimental tapers are shown.

A taper is fabricated in two steps:[20,50−53] Taper etching and coating of the new upper cladding. We have used two different masked RIE techniques to effect taper etching. The first method is oxygen-reactive ion etching with a shadow mask. The shadow mask is a 0.25 mm glass slide. It is attached with UV epoxy to a glass spacer which supports the shadow mask and defines the height of the shadow mask. The mask is placed on the sample and etching is carried out in a standard parallel plate (Plasma Technology Plasmlab) etcher at a pressure of 400 mTorr, radiofrequency power of 40 W, and 50 sccm oxygen flow rate. The shadow mask partially shields the sample underneath and also deflects the ion flux, causing a position-dependent etch rate in the vicinity of the end of the shadow mask. This leads to an S-shaped taper.

The second method for making the taper utilizes photolithography with a gray-scale mask, followed by reactive ion etching. A holographic plate is exposed with a computer-generated pattern which has a linear change of gray levels. After being developed and fixed, this holographic plate is used as a gray-scale photomask for patterning photoresist (Hoechst AZ5214E) spun onto the waveguide sample. The continuous change of exposure level in positive photoresist leads to a continuous change of photoresist thickness; therefore, a vertical taper of photoresist is formed. This vertical taper is then transferred into the waveguide upper cladding using regular oxygen-reactive ion etching. A linear taper is used in our experiment but other taper profiles can be obtained by changing the computer-generated gray-level pattern.

Both techniques worked well with our samples. Reactive ion etching with a shadow mask is easy to realize, but since the tail of the S-shaped taper decays gradually, the surface approximately 1 mm beyond the taper may still have some residue slope. This unwanted surface slope can cause difficulty in thickness control. Photolithography with a gray-scale mask requires more processing steps but provides better thickness uniformity after etching. In addition, the ability to control the taper profile with this method is useful in the further optimization of the shape of the taper.

An advantage of polymers is evident in satisfying the index of refraction requirements of the upper cladding used to overcoat the etched taper. Indices of refraction varying from 1.3 to 1.7 are readily obtained.[54] For our

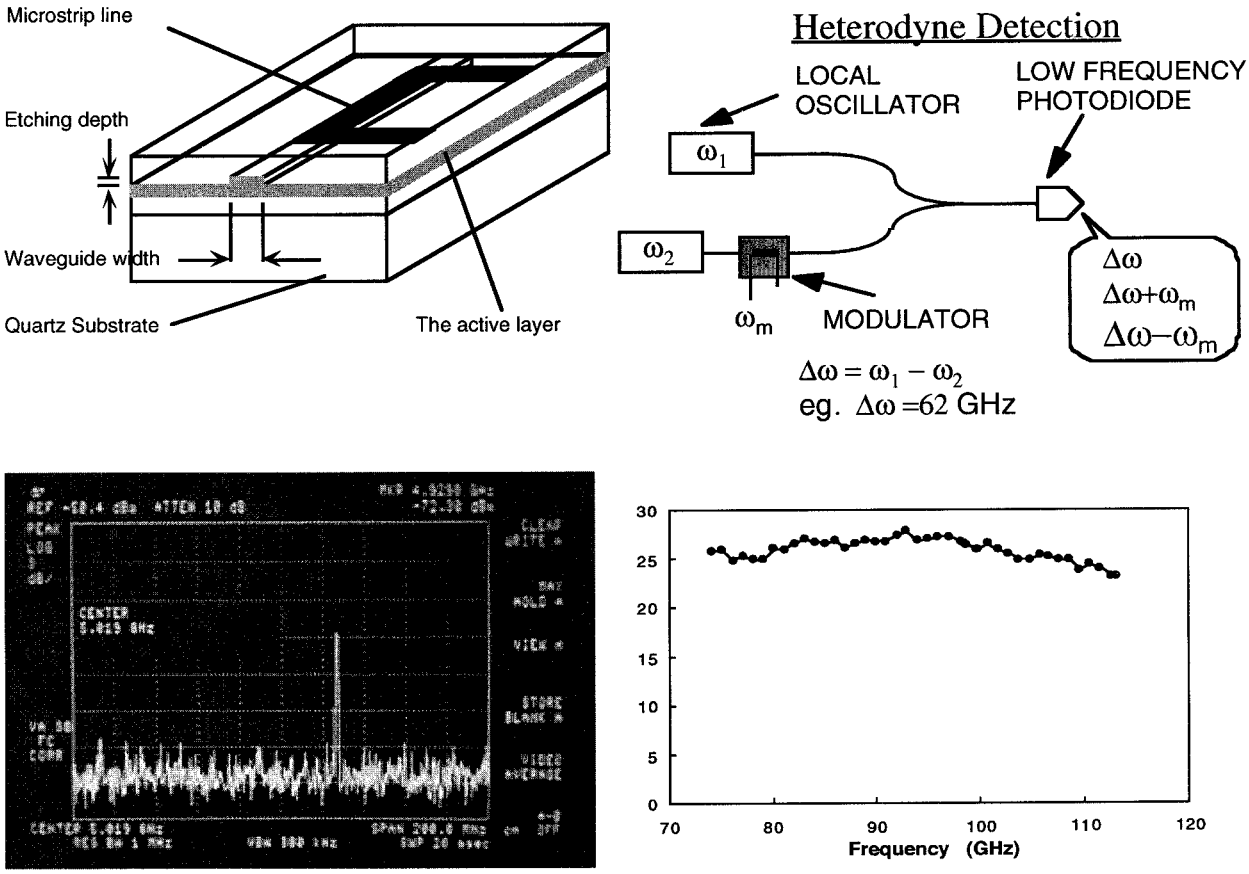

Figure 23. (Top) Schematic representations are given for a prototype birefringent modulator and the test bed used to evaluate its performance. (Bottom left) A spectrum analyzer trace showing 60 GHz modulation is shown. (Bottom right) The frequency dependence of the modulator output is shown from 75 to 113 GHz.

work, we use Cargille Labs MeltMounts which are thermoplastic polymeric materials with low optical loss at 1.3 μm. By mixing two MeltMounts of different indices, one can get any index in between.

We have found that reduction in optical loss using tapered mode size transformers is polarization-independent (comparable results are obtained for TE and TM modes). Experimentally observed reductions in coupling loss are in reasonable agreement with those of theory and the coupling loss has been reduced to less than 2 dB/coupling.

7. Review of Simple Device Configurations

The three most common basic configurations of polymeric modulators are the birefringent modulator, the Mach−Zender interferometer, and the directional coupler.[8] The birefringent modulator is a phase modulator which can be converted to an amplitude modulator by the addition of an input and output polarizer.

The Mach−Zender (MZ) interferometer consists of two straight waveguide sections as modulation areas and two Y-branches (one of which splits the optical beam into two beams and the other of which recombines the modulated beams back together). The modulating electric field is applied to one or both arms to modulate the phase of optical beams passing through these arms. When the two beams recombine at the second Y-branch, the phase difference between the two arms results in an amplitude modulation of the optical signal. In analogue signal applications, a dc bias voltage is applied to one arm to adjust the relative phases of the two arms in the absence of modulation. At a proper dc bias voltage and when the modulation signal is small, the output signal is linearly proportional to the input electrical signal with small third-order and higher odd-order harmonic distortion terms. A linearization scheme is required to correct for the third-order term. Either the third-order term must be subtracted from the output or a similar term must be added to the modulating electric field to cancel the distortion. Development of appropriate linearization is a current area of considerable importance in optochip development.

Directional couplers consist of two side-by-side waveguides separated by only a few microns. The overlap of the guided waves in the two waveguides couples energy back and forth between the waveguides. When an electrical voltage is applied, switching between the two output channels is obtained either by modulating the phase difference or the coupling coefficient of the two waveguides. Since the directional coupler has all orders of harmonic distortion terms, linearization must correct for both second and third-order distortions.

8. Prototype Device Evaluation

With the ability to fabricate low-loss buried channel polymeric electro-optic modulator waveguides and to efficiently couple light in to and out of these waveguides, the stage has been set for the fabrication and evaluation of simple prototype devices. In Figure 23, we show a simple stripline electrode (birefringent) modulator with an accompanying heterodyne test bed. A frequency analyzer trace showing 60 GHz modulation is presented at the bottom left and modulator performance from 75 to 113 GHz is illustrated at the bottom right. The slight

drop off of a modulation efficiency observed above 100 GHz is due to losses in the electrode structure and is not due to any bandwidth limitation of the polymeric electro-optic modulator material. This same modulator has been evaluated from dc to 113 GHz[55−58] and has been operated for extended periods of time at elevated temperatures and exposure to high optical power without degradation of performance.

The TACAN Corp. has investigated both birefringent and Mach−Zender modulators for CATV applications.[59] A carrier-to-noise ratio of 53 dB and an 80 channel television transmission has been demonstrated using packaged polymer modulators. A similar demonstration has been carried out by IBM researchers. TACAN has also investigated long-term half-wave voltage stability, dc bias voltage stability, and optical power handling capability. Polymeric modulators were observed to exhibit good halfwave voltage stability (e.g., no detectable change in V_π was observed over a period of a year in a typical long-term performance test). Polymeric modulators exhibit a relatively small dc bias voltage drift (e.g., less than 10% over a 120 h period); moreover, no "runaway" behavior (i.e., a continuous drift in one direction) was observed.

Photochemical stability is more difficult to discuss. Two mechanisms have been identified to account for instability of some EO polymers at high levels (>1 M/cm^2).[59−61] The first mechanism is reorientation of chromophores (e.g., containing azobenzene units) by photoinduced trans−cis−trans isomerization. The second mechanism involves photosensitized oxidation of chromophores. Results vary, as is to be expected, from chromophore to chromophore and with the nature of the polymer lattice (e.g., the degree of lattice hardening).[28,40,59−63] One of the most detailed studies of the photochemistry of active polymer waveguides is by R. Mustacich who is also pursuing the use of multiccolor lithography for the processing of waveguides (see earlier discussion).[40]

TACAN has tested photochemical stability over the spectral range from 543 to 1320 nm for PU-DR19[59] and related azobenzene chromophore based materials (e.g., LD-3[38,61]). Except for the anticipated photoinduced depoling effect at visible wavelengths observed for azobenzene chromophore containing materials,[59,61] polymeric modulators were quite stable. No instability was observed for low-power (e.g., 10 mW of 1.3 μm light) operation for long periods of time. Long-term operation at 150 mW power revealed a detectable degradation of performance for polymer modulators fabricated from PU-DR19 materials where only one end of the chromophore is attached to the polymer matrix.[63] No detectable degradation was observed for materials with both ends of the chromophore attached to the polymer lattice. Mustacich[62] and others[63] have observed that chromophores (e.g., the FTC chromophore discussed earlier) which do not undergo photoinduced conformational changes and which exist in heavily cross-linked lattices exhibit greatly improved photochemical stability relative to azobenzene chromophores. When oxygen is excluded from such chromophores, photochemically induced changes are no longer a relevant issue for device utilization (at least on the time scale of thousands of hours).[63]

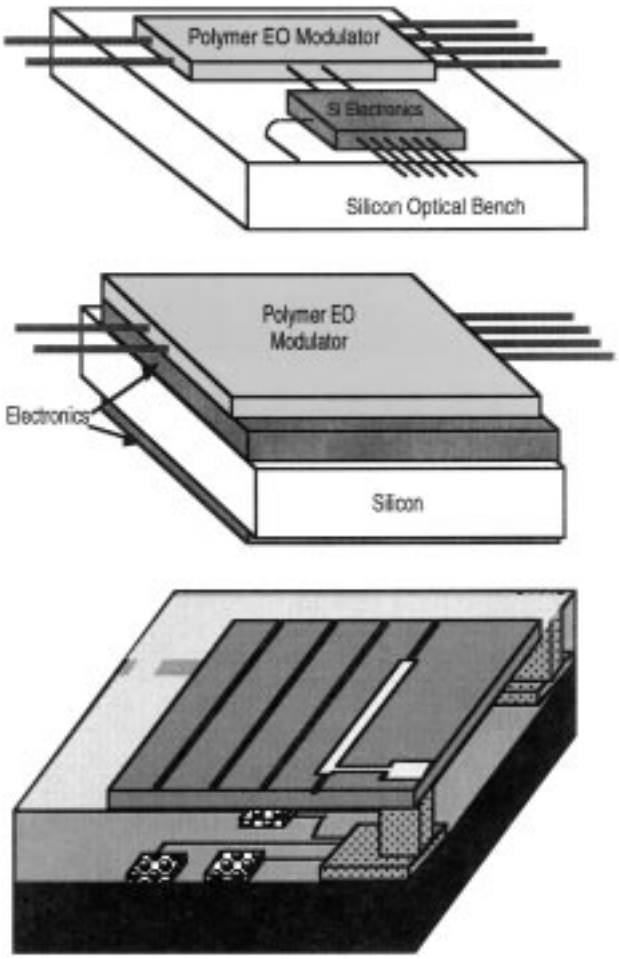

Figure 24. (Top) A schematic representation demonstrating horizontal (side-by-side) integration of a polymer electro-optic modulator with VLSI electronics is shown. (Middle) A schematic representation illustrating vertical integration is shown. (Bottom) A more detailed representation of the vertically integrated device discussed in the text is shown.

9. Integration with Semiconductor VLSI Electronics

If electro-optic modulators are to experience widescale application in telecommunications and signal processing, polymeric electro-optic modulators must be efficiently integrated with semiconductor electronics to create "optochips".[64] As can be seen from Figure 24, integration can be effected as either horizontal or vertical integration. Vertical integration has the advantage of the more efficient use of space (e.g., shorter interconnection lengths). However, vertical integration requires a more systematic development of an efficient integration (addressing issues of the nonplanar surface of VLSI circuitry, the problem of protecting VLSI circuitry during poling of the electroactive polymer, and the interconnect problem between VLSI circuitry and modulator electrodes).

The concept of circuit integration leverages off of well-established semiconductor integrated circuit (IC) technology and is practical because electro-optic polymers are compatible with IC fabrication technology. Vertical integration is based on the use of preprocessed VLSI wafers which contain signal processing circuits, linearizing circuits, and possibly infrared detectors and amplifiers. Vertical integration is challenging because optical waveguides must be fabricated on smooth sur-

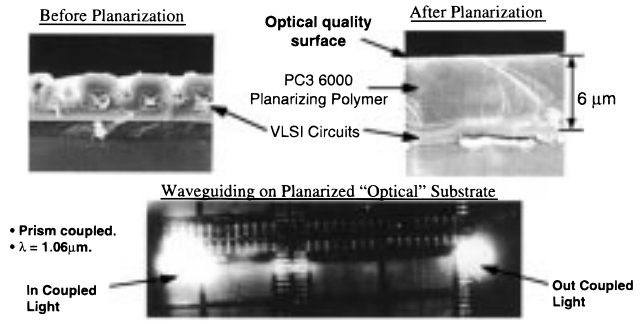

Figure 25. Planarization is illustrated together with a demonstration of optical waveguiding through the active polymer layer.

faces (since roughness of the surface of the substrate translates to the waveguides and results in high scattering losses); thus, global planarization of the surface topology of semiconductor circuits, to create optically smooth surfaces, becomes critical. Steier and co-workers[65−71] have used the planarizing polymer PC3-6000 (Futurrex) to achieve planarization. Since it is quite viscous compared to other polymers, some degree of planarization is achieved directly from spinning this material onto the VLSI wafer. At temperatures on the order of 200 °C, PC3-6000 reflows from the peaks to the troughs and further smoothes out the topology. Steier and co-workers[65−71] have shown that 1−6 μm semiconductor circuit features can be reduced to variations of 0.2 μm after planarization (see Figure 24). However, the real test of the success of planarization is the level of optical loss for modulator waveguides fabricated on the planarized surfaces. Steier and co-workers[65−71] have found that optical losses for waveguides fabricated on planarized VLSI wafer surfaces are less than 1 dB/cm which are indistinguishable from losses of waveguides fabricated on normal substrates (e.g., polished silicon). Thus, planarization is found to work surprisingly well.

The next question which must be answered is whether VLSI electronics can survive all phases of the integration process and most particularly corona poling of the electro-optic thin film fabricated on top of the VLSI circuitry. To answer this question, Steier and co-workers[65−71] have fabricated a birefringent polymeric electro-optic modulator on top of GaAs MESFET circuitry. The modulator design is that of Figure 23. The VLSI circuitry was planarized at 200 °C and then coated with a film of water-soluble poly(vinyl alcohol), chromium metal, and an electro-optical polymer. The chromium metal layer was used to realize the microstrip line electrode of the birefringent modulator and also functions as the ground plane for subsequent poling of the electro-optical polymer. This ground plane acts as a shielding layer to protect the underlying VLSI electronics. Corona poling was used by Steier and co-workers to induce acentric chromophore organization and thus electro-optic activity of the (PU-DR19) polymer layer. As is evident from a consideration of the MESFET current−voltage, I−V, curves (see Figure 26), the metal ground plane layer is critical to the protection of the MESFET electronics. With the chromium metal layer acting as a ground plane (shielding layer) for corona poling, the MESFET I−V curves are unchanged before and after poling. Fabrication of polymeric electro-optic modulator circuitry on top of VLSI semiconductor circuitry can be accomplished without detectable degradation of the performance of semiconductor electronics. Steier and co-workers[65−71] have established that the same is true for the electro-optic modulator circuit performance.

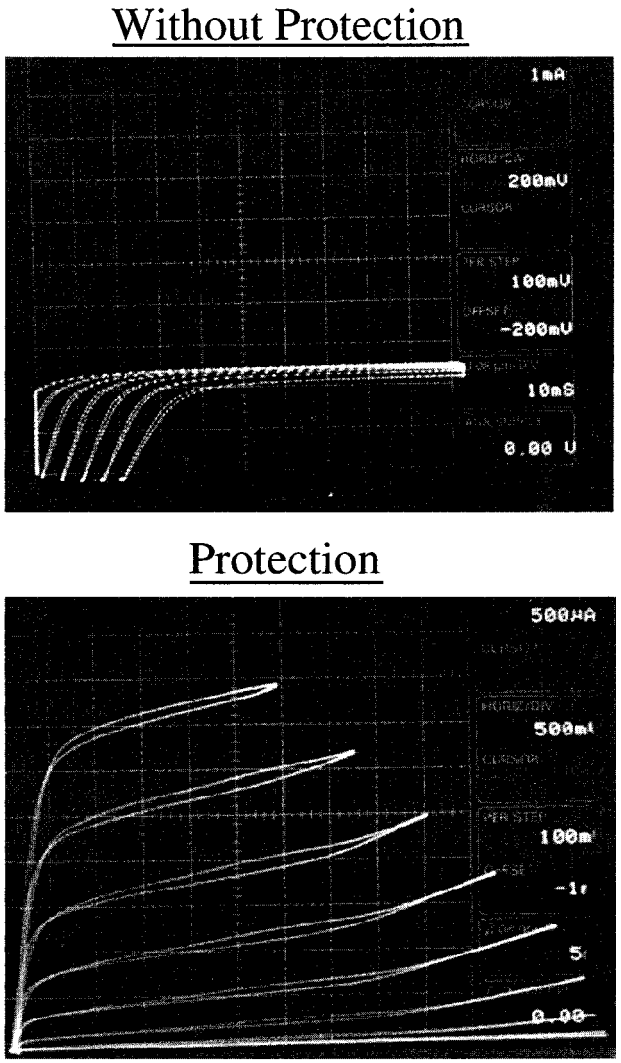

Figure 26. I−V curves for a MESFET device is shown for the fabrication of integrated devices carried out with and without protection of the VLSI electronics during corona poling.

The final challenge, which must be faced in the vertical integration of polymeric electro-optic modulators with semiconductor VLSI electronics, is that of interconnection of the two circuitries. This translates into the challenge of making vertical vias through thick polymer using a photoresist. We have accomplished this using trilayer processing (see Figure 27) and an oxygen RIE resistant material (spin on glass) to transfer the pattern (a normal photoresist is a poor mask for oxygen RIE of other polymers so we use spin-on glass). A perfluoromethane plasma is used to etch the spin on glass which is followed by oxygen plasma etching of the deep vias in the planarizing polymer and deposition of metal electrodes connecting to the VLSI circuitry.[65−71]

As a first step toward millimeter wave integration, a semiconductor power amplifier operating from 38 to 44 GHz was used with the birefringent phase modulator circuitry of Figure 23. The amplifier was an InGaAs high-electron mobility transistor microwave monolithic integrated circuit (MMIC) with a 12 dB single-stage gain. Using a low-power source and two of the millimeter wave amplifiers, a signal-to-noise ratio at the output of the polymer phase modulator of over 40 dB

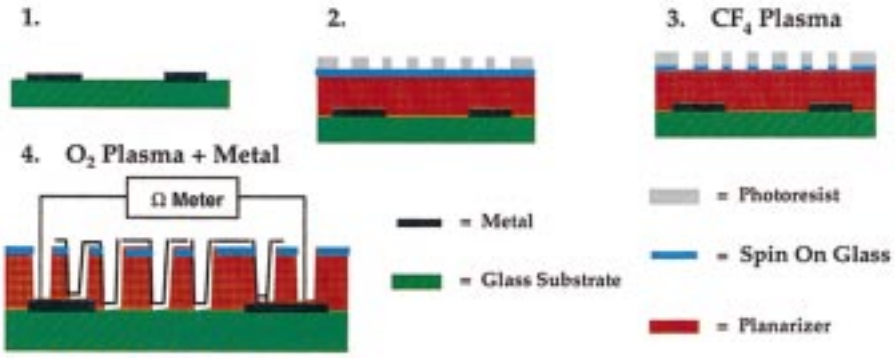

Figure 27. The fabrication of deep vias for a modulator−VLSI interconnection is shown.

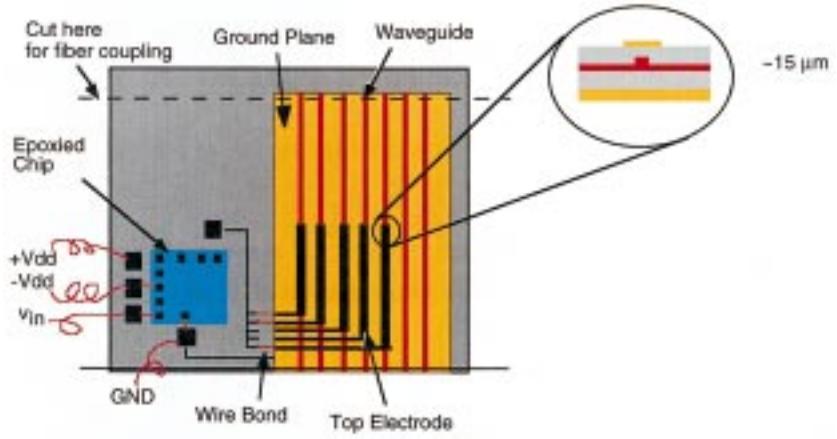

Figure 28. An optochip prepared using side-by-side integration is shown.

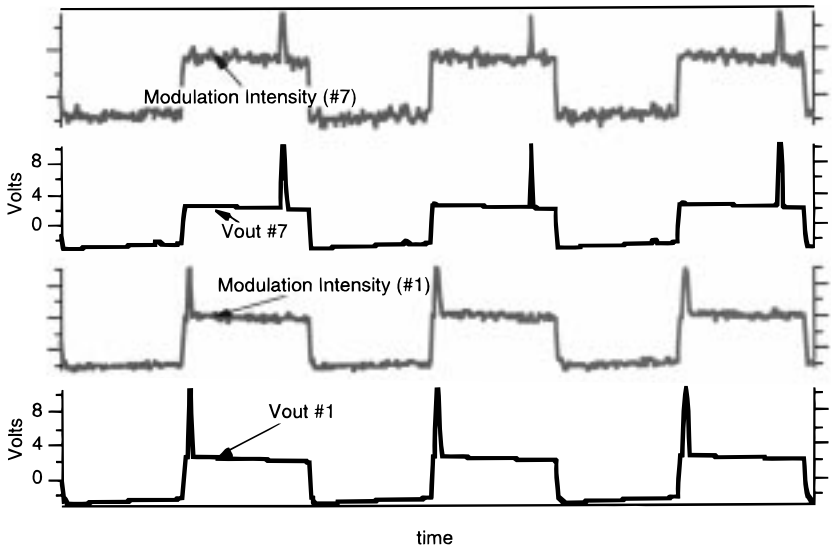

Figure 29. Optochip performance is demonstrated. Two output signals drive modulators 1 and 7. The modulator output is shown above the corresponding electrical driver signal.

was easily obtained. This demonstrates that MMIC devices are easily capable of driving polymeric modulators.

10. Organic Optochips

It is desirable to use multiple signals (outputs) from a single VLSI chip to drive multiple electro-optic modulators (optochips). We have demonstrated that many polymeric waveguide modulators can be fabricated on a single wafer with 100% yield (all modulators operating within specifications).[28,67,71] Recently, we have demonstrated optochip performance employing side-by-side integration. Side-by-side integration was chosen because of the space requirements of our multiple modulator array.

In Figure 28, we show an optochip structure which we have fabricated and evaluated (see Figure 29). In Figure 29, we show two outputs from our semiconductor driver chip driving electro-optic modulators 1 and 7. It is clear that the electrical voltage information is encoded on the optical transmission through these waveguides with no noticeable distortion. We have evaluated modulator packages to the frequency limits of the VLSI

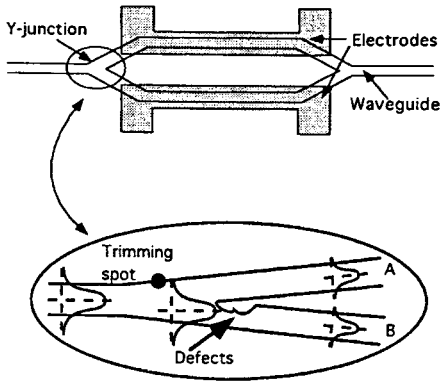

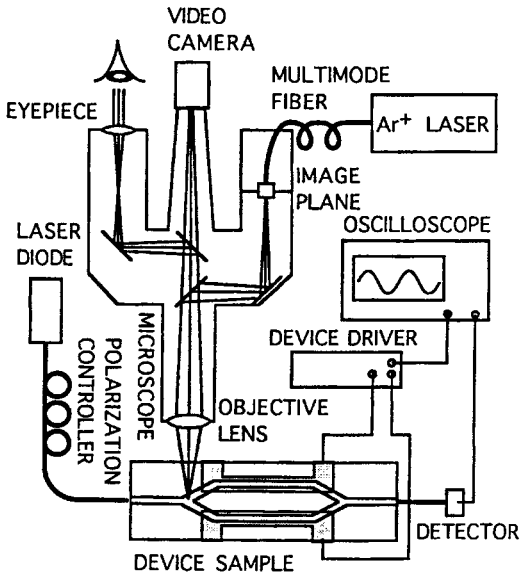

Figure 30. Trimming is schematically illustrated.

electronics which provide the drive voltages for the polymeric modulators. In this simple device, no crosstalk between adjacent modulators was observed; however, this is an issue that merits careful evaluation for a variety of multimodulator packages before it is assumed to be unimportant. However, this cautionary comment should not detract from the observation that to this point in time integration of polymeric modulators with VLSI electronics appears very promising indeed.

11. Trimming for Tuning Device Specifications

For waveguide devices, imperfections can seriously affect device performance such as the splitting ratio of Y-junction splitters, the extinction ratio of Mach−Zender modulators, and the coupling constant of directional coupler switches. Trimming techniques which can tune device performance will reduce device cost, improve performance, and increase fabrication yield.[28,72−74] For waveguide devices containing photobleachable chromophores (e.g., a Mach−Zender modulator fabricated from PU-DR19) postfabrication in situ trimming can be employed to improve performance.[28,72−74]

We have used such trimming with a Mach−Zender modulator (see Figure 30). The principal can be explained as follows: Suppose that the fabricated power splitting Y-junction of the MZ modulator exhibits imbalanced output powers because of defects in the waveguide. The power imbalance causes a lower extinction ratio. Photobleaching the side of the waveguide branch which receives more power immediately before the splitting point or after the recombining point will reduce the refractive index of that area which will in turn shift the mode peak away from the trimmed side. This is equivalent to a horizontal realignment of the waveguide mode before the Y-junction. The power in the two MZ arms can be balanced without inducing excess loss. Since the trimming is made outside the active (electro-optic modulation) waveguide section, the electro-optic properties of the device are not affected by trimming. For in situ trimming, the device should be operated and the on−off ratio monitored during the process.

As can be seen from Figure 30, a trimming setup is relatively simple. Light from a 488 nm argon ion laser

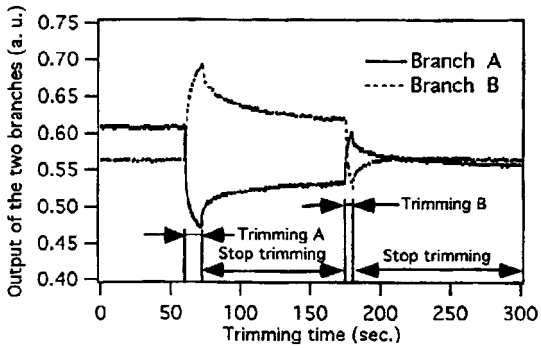

Figure 31. The experimental trimming of a Mach−Zender PU-DR19 modulator is shown.

is delivered by a multimode fiber. One eyepiece of a modified binocular microscope is removed and the output end of the fiber is place in the image plane of the objective lens. The microscope objective reduces the output pattern of the fiber and projects the reduced image onto the sample. The size of the spot is determined by the fiber core size, the magnifying power of the microscope objective lens, and the axial position of the tip of the fiber. A spot size from 1 μm to >1 mm on the waveguide sample is obtainable. The position of the spot on the sample is observed through the other eyepiece or by a video camera on the microscope. Because the fiber tip is fixed to the microscope, its image always appears at the same place in the observation field of view when moving the microscope. This arrangement makes it very simple to position the beam spot to where photobleaching should be performed.

In Figure 31, we show the change in output power from the two branches of a Mach−Zehnder Y-junction under trimming. The branch which is being photobleached loses power because of a reduced refractive index and the other branch gains power. The splitting ratio is therefore changed. Trimming the other branch changes the ratio in the opposite direction. This error correction capability makes the technique fault-tolerant. In our experiment, the splitting ratio could be tuned ±20% for the TE mode and ±10% for the TM mode. The change of the total output power from the two branches is less than 0.2 dB after repeated trimming of the two branches. The fast partial recovery of the splitting ratio

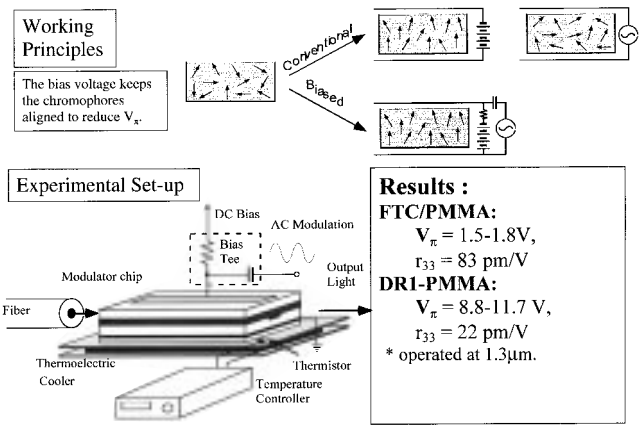

Figure 32. The principles of operation with and without a dc bias voltage are illustrated. Also shown is a schematic of the device configuration used for biased operation of EO polymer modulators.

after the trimming light is turned off can be explained by the fast relaxation of the cis−trans isomerization and the thermooptical effect. Over-trimming and multiple trimming sessions can be used to compensate this partial recovery and to reach the required splitting ratio. The power of the unpolarized trimming beam incident on the sample is only a few microwatts. Since the power is focused on a small spot, the power density in the trimming spot is still very high. The time required to trim a device is only on the order of 10 s which is very short compared to conventional masked photobleaching trimming which takes several hours to complete. Since trimming can be accomplished exploiting photodecomposition (e.g., oxidation) of chromophores, trimming may prove applicable to a wide range of organic nonlinear optical materials.

12. Realizing the Full Potential of Electro-optic Chromophores

Electro-optic modulation is routinely performed without the application of a dc bias field (see Figure 32). Without utilization of a bias voltage, the electro-optic activity is always attenuated relative to that obtained during electric field poling because of relaxation of the acentric order (both due to chromophore reorientation and the dissipation of surface charge). It is conceivable that applications of electro-optic materials may arise in the future which can take advantage of the greater electro-optic activity which can be achieved by application of a bias field (see Figure 32). Thus, we have begun to systematically explore not only electro-optic activity in conventional device configurations which operate in the absence of a bias field but also electro-optic activity utilizing the configuration shown in Figure 32 which employs a bias field.[18,19,28] This particular configuration has the advantage of avoiding problems associated with acentric order stabilization by lattice hardening including the problem of optical loss arising from postpoling lattice hardening and inhibition of poling-induced reorientation due to premature cross-linking.

The FTC/PMMA solid solutions, which gave electro-optic coefficients on the order of 50 pm/V in the absence of a dc bias field (the only applied electric field being the modulation or ac field), give electro-optic coefficients on the order of 80 pm/V with application of a bias field of 300 V (60 V/μm). The 80 pm/V electro-optic coefficient obtained for FTC/PMMA with this bias field is equal to that obtained for the isophorone-protected, polyene analogue of FTC without a bias even though the molecular optical nonlinearity of the latter is considerably larger (see Table 3). In a like manner, DR1/PMMA solid solutions yield electro-optic coefficients on the order of 22 pm/V with a dc bias field and electro-optic coefficients on the order of 13 pm/V without a bias field.

Because attenuation of optical nonlinearity from various mechanisms (except obvious mechanisms such as chemical reaction, electrical conductivity, and photoconductivity) do not affect the experiments with the bias field, we refer to such experiments as assessing the full potential of nonlinear optical chromophores. This gives useful target figures, both in terms of electro-optic coefficients and optical loss, to shoot for with optimized chromophore processing (poling and lattice hardening) conditions. If bias fields can be employed in future devices, it is clear that V_π voltages of 1 V can be obtained with the best currently available chromophores and that optical loss of 1 dB/cm (or slightly less) can be anticipated.

13. Future Prognosis

Many putative advantages of polymeric modulators have been demonstrated in the past 2 years including a modulation bandwidth of greater than 100 GHz (a current record for any material), electro-optic coefficients comparable to or greater than that of lithium niobate, successful integration with semiconductor VLSI electronics and with silica fibers, reasonable performance in field tests of prototype devices, and optochip (multimodulator) operation. The stage has been set for the limited commercialization of polymeric modulators for niche applications. For a wider application, further improvements in materials properties and in device design (e.g., response linearization, utilization of faster drivers, etc.) must be made.

The most serious materials property is probably that of optical loss. Many applications require very low loss (e.g., waveguide loss of 0.1 dB/cm or less and coupling losses of less than 1 dB). While such losses may be possible with organic (polymeric) materials, realization will require the minimization of chromophore absorption at operational wavelengths (with a minimum sacrifice of optical nonlinearity), minimization of optical absorption by the host polymer, and minimization of scattering (processing) losses. Almost certainly, no single chromophore/polymer material will be the material of choice for all applications. Particular areas of focus required for improved transparency include development of "blue-shifted" high $\mu\beta$ chromophores, fluorination to reduce losses from C−H vibrations for infrared operational wavelengths, and development of hardened active waveguide materials resistant to solvent damage to underlying polymer layers during subsequent spin-coating operations (e.g., the electro-optic core can be damaged by spinning on the upper cladding layer, and any layer can be damaged by spinning on or removing of a photoresist layer). This latter problem may be one of the most difficult to solve for device fabrication by RIE methods but is a problem which should ultimately be amenable to solution by chemists.

If disperse red and DANS chromophore/polymer materials are considered the "first-generation" second-order nonlinear optical materials, then we are entering a period where second-generation materials are beginning to be used for prototype device fabrication. Many new problems such as chromophore aggregation are

being encountered and each problem must be systematically addressed. New chromophores require reinvestigation of concepts of lattice hardening developed for disperse red and DANS-type materials. As many new chromophores do not undergo photoinitiated conformational changes, these new chromophores cannot be used with multiccolor photolithography unless photochromic moieties are also incorporated into the polymer or unless one relies on index change due to photodecomposition (oxidation). Of course, optimum RIE and ECR processing conditions will have to be defined for each new material.

Another critical issue is that of adapting processing techniques and protocols to the fabrication of large-scale devices. Steier and co-workers have carried out spin casting and poling operations leading to acceptably uniform electro-optic polymer materials on a 6 in. semiconductor wafer. Large-scale devices would require different processing techniques than those currently used (e.g., multiple electrode poling or the realization of acentric order by techniques (molecular self-assembly) which do not require electric field poling).[1,8,9,35]

The exploitation of integrated device technology may require finding faster semiconductor drivers than those currently available.

What are some of the potential applications of polymeric electro-optic modulators? Certainly, there is high-speed optical switching in local area network nodes using materials in a directional coupler configuration. There are electrical-to-optical signal transduction operations as in the cable television industry, for back-plane interconnections between high-speed parallel processors (digital computers), voltage sensing (e.g., at power transformers) in the electrical power industry, photonic detection of electrical fields and electromagnetic radiation (e.g., photonic detection of radar, in analytical and biomedical applications, etc.), phased array radar, gyroscopes, and Gbit/s analog-to-digital conversion (e.g., optical folding-flash A−D conversion). Selected small-angle beam steering applications may also be feasible in certain flat panel display applications. In some applications such as satellite telecommunications, features such as low weight (easily afforded by polymers) may even enter into consideration in promoting the use of polymers.

Acknowledgment

The authors thank Professors William H. Steier (USC), Harold R. Fetterman (UCLA), and their students for invaluable contributions to the work reviewed here and for numerous enlightening discussions. Discussions with Dr. Charles Lee motivated a number of experiments and his insights are acknowledged. The authors gratefully acknowledge financial support from the Air Force Office of Scientific Research (F49620-96-1-0185, F49620-97-1-0307, and F49620-97-1-0491) and from the National Science Foundation (DMR-9528021).

Literature Cited

(1) Dalton, L. R.; Harper, A. W.; Ghosn, R.; Steier, W. H.; Ziari, M.; Fetterman, H.; Shi, Y.; Mustacich, R. V.; Jen, A. K. Y.; Shea, K. J. Synthesis and Processing of Improved Organic Second-Order Nonlinear Optical Materials for Applications in Photonics. *Chem. Mater.* **1995**, *7*, 1060 and references contained therein.

(2) Prasad, P. N.; Williams, D. J. *Introduction to Nonlinear Optical Effects in Molecules and Polymers*; Wiley: New York, 1991.

(3) Dalton, L. R. Nonlinear Optical Materials. In *Kirk−Othmer Encyclopedia of Chemical Technology*, 4th ed.; Kroschwite, J. I., Howe-Grant, M., Eds.; Wiley: New York, 1996; Vol. 17, p 287.

(4) Agrawal, G. P.; Flytzanis, C. Delocalization and Superalternation Effects in the Nonlinear Susceptibilities of One-Dimensional Systems. *Chem. Phys. Lett.* **1976**, *44*, 366.

(5) Heflin, J. R.; Wong, K. Y.; Zamani-Kharmiri, O.; Garito, A. F. Nonlinear Optical Properties of Linear Chains and Electron-Correlation Effects. *Phys. Rev. B* **1988**, *38*, 1573.

(6) Kanis, D. R.; Ratner, M. A.; Marks, T. J. Design and Construction of Molecular Assemblies with Large Second-Order Optical Nonlinearities. Quantum Chemical Aspects. *Chem. Rev.* **1994**, *94*, 195.

(7) Youmans, A. P.; Rose, R. E.; Greeman, W. F. Multichip Packages Utilizing In−Cu Flip-Chip Bonding. *IEEE Proc.* **1969**, *57*, 1599; Gorski, D. A.; Zappella, P. I.; Asch, A. E. Flip-Chip Header for IR Detector Arrays Operating at Cryogenic Temperatures. *IEEE Trans. Parts, Hybrids Packaging* **1975**, PHP-11, 312.

(8) Dalton, L. R.; Harper, A. W.; Wu, B.; Ghosn, R.; Laquindanum, J.; Liang, Z.; Hubbel, A.; Xu, C. Polymeric Electro-optic Modulators: Materials Synthesis and Processing. *Adv. Mater.* **1995**, *7*, 519.

(9) Dalton, L. R.; Sapochak, L. S.; Chen, M.; Yu, L. P. Ultrastructure Concepts of Optical Integrated Microcircuits and Polymeric Materials. In *Molecular Electronics and Molecular Electronic Devices*, Sienicki, K., Ed.; CRC Press: Boca Raton, FL, 1993; p 125.

(10) Jen, A. K. Y.; Cai, Y.; Bedworth, P. V.; Marder, S. R. Synthesis and Characterization of Highly Efficient and Thermally Stable Diphenylamino-Substituted Thiophene Stilbene Chromophores for Nonlinear Optical Applications. *Adv. Mater.* **1997**, *9*, 132 and references contained therein.

(11) Harper, A. W. Systematic Optimization of Second-Order Optical Nonlinearities in Molecules and Polymers. Ph.D. Thesis, University of Southern California, Los Angeles, CA, 1997.

(12) Cheng, L. T.; Tam, W.; Marder. S. R.; Stiegman, A. E.; Rikken, G.; Spangler, C. W. Experimental Investigations of Organic Molecular Nonlinear Optical Polarizabilities. 2. A Study of Conjugation Dependences. *J. Phys. Chem.* **1991**, *95*, 10643.

(13) Clays, K.; Persoons, A. Hyper-Rayleigh Scattering in Solution. *Phys. Rev. Lett.* **1991**, *66*, 2980.

(14) London, F. The General Theory of Molecular Forces. *Trans. Faraday Soc.* **1937**, *33*, 8.

(15) Dalton, L. R.; Harper, A. W.; Robinson, B. H. The Role of London Forces in Defining Noncentrosymmetric Order of High Dipole Moment−High Hyperpolarizability Chromophores in Electrically Poled Polymeric Thin Films. *Proc. Natl. Acad. Sci. U.S.A.* **1997**, *94*, 4842.

(16) Harper, A. W.; Sun, S.; Dalton, L. R.; Garner, S. M.; Chen, A.; Kalluri, S.; Steier, W. H.; Robinson, B. H. Translating Microscopic Optical Nonlinearity to Macroscopic Optical Nonlinearity: The Role of Chromophore−Chromophore Electrostatic Interactions. *J. Opt. Soc. Am. B* **1998**, *15*, 329.

(17) Chen, J.; Zhu, J.; He, M.; Dalton, L. R.; Garner, S.; Chen, A.; Steier, W. H. High E−O Coefficient Polymers Based on a Chromophore Containing Isophorone Moiety for Second-Order Nonlinear Optics. *Mater. Res. Soc. Symp. Proc.* **1998**, *488*, 151; Chen, J. Design, Synthesis and Characterization of Second-Order Nonlinear Optical Chromophores and Their Related Polymers. Ph.D. Thesis, University of Southern California, Los Angeles, CA, 1998.

(18) Chen, A.; Chuyanov, V.; Zhang, H.; Garner, S.; Steier, W. H.; Chen, J.; Zhu, J.; He, M.; Mao, S. S. H.; Dalton, L. R. Demonstration of the Full Potential of Second-Order Nonlinear Optic Polymers for Electro-optic Modulation Using a High $\mu\beta$ Chromophore and a Constant Bias Field. *Opt. Lett.* **1998**, *23*, 478.

(19) Chen, A.; Chuyanov, V.; Zhang, H.; Garner, S.; Lee, S.-S.; Steier, W. H.; Chen, J.; Zhu, J.; Wang, F.; He, M.; Ra, Y.; Mao, S. S. H.; Dalton, L. R.; Fetterman, H. R. Low V_π Electro-optic Polymer Waveguide Modulators Using the Full Potential of High $\mu\beta$ Chromophores and a Constant Bias Voltage. *Proc. SPIE* **1998**, *3281*, 10.

(20) Wang, F. Design, Synthesis, and Characterization of Novel Organic Chromophores and Polymers for Electro-optic Modulation. Ph.D. Thesis, University of Southern California, Los Angeles, CA, 1998.

(21) Teng, C. C.; Man, H. T. Simple Reflection Technique for Measuring the Electro-optic Coefficient of Poled Polymers. *Appl. Phys. Lett.* **1990**, *56*, 1734.

(22) Levy, Y.; Dumont, M.; Chastaing, E.; Robin, P.; Chollet, P. A.; Gadret, G.; Kajzar, F. Reflection Method for Electro-optical Coefficient Determination in Statified Thin Film Structures. *Mol. Cryst. Liq. Cryst. Sci. Technol., Sect. B* **1993**, *4*, 1.

(23) Dentan, V.; Levy, Y.; Dumont, M.; Robin, P.; Chastaing, E. Electro-optic Properties of a Ferroelectric Polymer Studied by Attenuated Total Reflection. *Op. Commun.* **1989**, *69*, 379.

(24) Ziari, M.; Kalluri, S.; Garner, S.; Steier, W. H.; Liang, Z.; Dalton, L. R.; Shi, Y. Novel Electro-optic Measurement Technique for Coplanar Electrode Poled Polymers. *Proc. SPIE* **1995**, *2527*, 218.

(25) Kalluri, S.; Garner, S.; Ziari, M.; Steier, W. H.; Shi, Y.; Dalton, L. R. Simple Two-Slit Interference electro-optic Coefficients Measurement Technique and Efficient Coplanar Electrode Poling of Polymer Thin Films. *Appl. Phys. Lett.* **1996**, *69*, 275.

(26) Becker, M. W.; Sapochak, L. S.; Ghosn, R.; Xu, C.; Dalton, L. R.; Shi, Y.; Steier, W. H.; Jen, A. K. Y. Large and Stable Nonlinear Optical Effects Observed for a Polyimide Covalently Incorporating a Nonlinear Optical Chromophore. *Chem. Mater.* **1994**, *6*, 104.

(27) Chen, A.; Chuyanov, V.; Garner, S.; Steier, W. H.; Dalton, L. R. Modified Attenuated Total Reflection for the Fast and Routine electro-optic Measurements of Nonlinear Optical Polymer Thin Films. In *Organic Thin Films for Photonic Applications, Vol. 14*; Optical Society of America: Washington, DC, 1997; p 158.

(28) Chen, A. Electro-optic Polymer Technologies and Devices for Applications in Photonics. Ph.D. Thesis, University of Southern California, Los Angeles, CA, 1998.

(29) Teng, C.-C. Precision Measurements of the Optical Attenuation Profile Along the Propagation Path in Thin-Film Waveguides. *Appl. Opt.* **1993**, *32*, 1051.

(30) Liang, Z.; Dalton, L. R.; Garner, S. M.; Kalluri, S.; Chen, A.; Steier, W. H. A Cross-Linkable Polyimide for Second-Order Optical Nonlinearites. *Chem. Mater.* **1995**, *7*, 941.

(31) Liang, Z.; Dalton, L. R.; Garner, S. M.; Kalluri, S.; Chen, A.; Steier, W. H. A Heterocyclic Polymer with Thermally Stable Second-Order Optical Nonlinearity. *Chem. Mater*, **1995**, *7*, 1756.

(32) Mao, S. S. H.; Ra, Y.; Guo, L.; Zhang, C.; Dalton, L. R.; Chen, A.; Garner, S.; Steier, W. H.; Progress Toward Device-Quality Second-Order Nonlinear Optical Materials. 1. Influence of Composition and Processing Conditions on Nonlinearity, Temporal Stability, and Optical Loss. *Chem. Mater.* **1998**, *10*, 146.

(33) Teng, C. C.; Mortazavi, M. A.; Boughoughian, G. K. Origin of Poling-Induced Optical Loss in a Nonlinear Optical Polymeric Waveguide. *Appl. Phys. Lett.* **1995**, *66*, 667.

(34) Nalwa, S. W.; Miyata, S. *Nonlinear Optics of Organic Molecules and Polymers*; CRC Press: Boca Raton, FL, 1997.

(35) Wise, D. L.; Wnek, G. E.; Trantolo, D. J.; Cooper, T. M.; Gresser, J. D. *Electrical and Optical Polymer Systems*; Marcel Dekker: New York, 1998.

(36) Oviatt, H. W., Jr.; Shea, K. J.; Kalluri, S.; Shi, Y.; Steier, W. H.; Dalton, L. R. Applications of Organic Bridged Polysilsesquioxane Xerogels to Nonlinear Optical Materials by the Sol−Gel Methods. *Chem. Mater.* **1995**, *7*, 493.

(37) Kalluri, S.; Steier, W. H.; Yang, Z.; Xu, C.; Wu, B.; Dalton, L. R.; Shi, Y.; Bechtel, J. H. Enhancement of Electro-optic Properties and Temperature Stability in Sol−Gel Polymer Thin Films. *Proc. SPIE* **1994**, *2285*, 131.

(38) Xu, C.; Wu, B.; Todorowa, O.; Dalton, L. R.; Shi, Y.; Ranon, P. M.; Steier, W. H. Stabilization of the Dipole Alignment of Poled Nonlinear Optical Polymers by Ultrastructure Synthesis. *Macromolecules* **1993**, *26*, 5303.

(39) Burland, D. M.; Miller, R. D.; Walsh, C. A. Second-Order Nonlinearity in Poled-Polymer Systems. *Chem. Rev.* **1994**, *94*, 31.

(40) It is not strictly true that a material which undergoes a photoinduced conformational change is a prerequisite for MCP. RVM Scientific (Santa Barbara, CA), which is seeking to commercialize scanning MCP, has produced buried channel waveguide structures utilizing photoinduced material damage (e.g., photosensitized oxidation), which changes the index of refraction. RVM Scientific has also carried out detailed investigations of the subtleties of photochemical processing and material evolution under high levels of light exposure at various wavelengths. For example, they have identified which processes produce index changes with and without inducing changes in birefringence (e.g., photoinduced oxidation vs photoinduced reorientation). RVM Scientific has also carried out detailed studies of the relationship of lattice hardness (polymer cross-linking) to photochemical kinetics.

(41) Chon, J. C.; Thackara, J. I.; Commita, P. B.; Jurich, M. C.; Swalen, J. D. Characterization of Low Loss Polymer Modulators Fabricated by Laser Ablation. *Proc. SPIE* **1994**, *2285*, 340.

(42) Franke, H.; Sterkenburgh, T. Pattering Polymer Surfaces by Laser Ablation for Integrated Optics. *Proc. 4th Int. Conf. Prop. Appl. Dielectric Mater.* **1994**, *1*, 208.

(43) Steier, W. H.; Kalluri, S.; Chen, A.; Garner, S.; Chuyanov., V.; Ziari, M.; Shi, Y.; Fetterman, H.; Jailai, B.; Wang, W.; Chen, D.; Dalton, L. R. Applications of Electro-optic Polymers in Photonics. *Mater. Res. Soc. Symp. Proc.* **1996**, *413*, 147.

(44) Chen, A.; Kaviani, K.; Remple, A.; Kalluri, S.; Steier, W. H.; Shi, Y.; Liang, Z.; Dalton, L. R. Optimized Oxygen Plasma Etching of Polyurethane Based electro-optic Polymers for Low Loss Waveguide Fabrication. *J. Electrochem. Soc.* **1996**, *143*, 3648.

(45) A speciality silica fiber of reduced and tapered dimensions does exist which can reduce the coupling problem somewhat.

(46) Bean, K. E. Anisotropic Etching of Silicon. *IEEE Trans. Electron Devices* **1978**, *ED-25*, 1185.

(47) Tabata, O.; Asahi, R.; Funabashi, H.; Shimaoka, K.; Sugiyama, S. Anisotropic Etching of Silicon in TMAH Solutions. *Sens. Actuators A* **1992**, *A34*, 51.

(48) Cohen, M. S.; Cina, M. F.; Bassous, E.; Opyrsko, M. M.; Speidell, J. L.; Canora, F. J.; DeFranza, M. J. Packing of High-Density Fiber/Laser Modules Using Passing Alignment Techniques. *IEEE Trans. Compon., Hybrids, Manuf. Technol.* **1992**, *15*, 944.

(49) Armiento, C. A.; Negri, A. J.; Tabasky, M. J.; Boudreau, R. A.; Rothman, M. A.; Fitzgerald, T. W.; Haugsjaa, P. O. Gigabit Transmitter Array Modules on Silicon Waferboard. *IEEE Trans. Compon., Hybrids, Manuf. Technol.* **1992**, *15*, 1072.

(50) Chen, A.; Chuyanov, V.; Marti-Carrera, F. I.; Garner, S.; Steier, W. H.; Chen, J.; Sun, S.; Dalton, L. R. Integrated Polymer Waveguide Mode Size Transformer with a Vertical Taper for Improved Fiber Coupling. *Proc. SPIE* **1997**, *3005*, 65.

(51) Chen, A.; Chuyanov, V.; Marti-Carrera, F. I.; Garner, S.; Steier, W. H.; Chen, J.; Sun, S.; Mao, S. S. H.; Ra, Y.; Dalton, L. R. Vertical Tapered Mode Size Transformer in Polymer Waveguides for Efficient Fiber Coupling. *Technical Digest of the Organic Thin Films for Photonic Applications, 1997 OSA Technical Digest Series* **1997**, *14*, 8.

(52) Chen, A.; Marti-Carrera, F. I.; Garner, S.; Chuyanov, V.; Steier, W. H. Fabrication of Vertical Tapers in Polymer Thin Films by Oxygen Reactive Ion Etching with a Shadow Mask for Photonic Device Applications. *Technical Digest of the Organic Thin Films for Photonic Applications, 1997 OSA Technical Digest Series* **1997**, *14*, 152.

(53) Chen, A.; Ziari, M.; Steier, W. H. Passive Alignment of Optic Fiber Array Using Silicon V-Grooves Monolithically Integrated with Polymer Waveguide Devices. *Tech. Digest Org. Thin Films Photonic Appl., 1997 OSA Tech. Digest Ser.* **1997**, *14*, 167.

(54) Seferis, J. C. Refractive Indices of Polymers. In *Polymer Handbook*, 3rd ed.; Brandrup, J., Immergut, E. H., Eds.; Wiley: New York, 1989; Vol. 1, p 451.

(55) Chen, D.; Fetterman, H. R.; Chen, A.; Steier, W. H.; Dalton, L. R.; Wang, W.; Shi, Y. High-Bandwidth Polymer Modulators. *Proc. SPIE* **1997**, *3006*, 314.

(56) Chen, D.; Fetterman, H. R.; Chen, A.; Steier, W. H.; Dalton, L. R.; Wang, W.; Shi, Y. Demonstration of 110 GHz Electro-Optic Polymer Modulators. *Appl. Phys. Lett.* **1997**, *70*, 3335.

(57) Chen, D.; Fetterman, H. R.; Tsap, B.; Chen, A.; Steier, W. H.; Dalton, L. R. High-Bandwidth Polymer Modulators. *Proc. LEOS'97* **1997**, *2*, 248.

(58) Chen, D. High-Speed Polymer Modulators. Ph.D. Thesis, University of California—Los Angeles, Los Angeles, CA, 1997.

(59) Shi, Y.; Wang, W.; Bechtel, J. H.; Chen, A.; Garner, S.; Kalluri, S.; Steier, W. H.; Chen, D.; Fetterman, H. R.; Dalton, L. R.; Yu, L. Fabrication and Characterization of High-Speed Polyurethane-Disperse Red 19 Integrated Electro-Optic Modulators for Analog System Applications. *IEEE J. Quantum Electron.* **1966**, *2*, 289.

(60) Mortazavi, M. A.; Yoon, H. N.; Teng, C. C. Optical Power Handling Properties of Polymeric Nonlinear Optical Waveguides. *J. Appl. Phys.* **1993**, *74*, 4871.

(61) Shi, Y.; Wang, W.; Lin, W.; Olson, D. J.; Bechtel, J. H. Double-End Crosslinked Electro-Optic Polymer Modulators with High Optical Polymer Handling Capability. *Appl. Phys. Lett.* **1997**, *70*, 1342.

(62) Mustacich, R. V., private communication.

(63) Dalton, L. R.; Strohkendl, F.; Axenson, T., unpublished data. For a chromophore to be considered for electro-optic device fabrication, it must obviously be largely free from photochemical mechanisms such as photoinduced (one- or two-photon) oxidation. Thus, the chromophores that we have evaluated over the past 2 years have already been heavily screened by detailed (including femtosecond) spectroscopic studies. Our remarks concerning photochemical stability apply only to this small subclass of organic chromophores.

(64) Mohlmann, G. R. Polymeric Optochips—Splitters, Switches, and Modulators. *Synth. Met.* **1994**, *67*, 77.

(65) Kalluri, S.; Chen, A.; Chuyanov. V.; Ziari, M.; Steier, W. H.; Dalton, L. R. Integration of Polymer electro-optic Devices on Non-Planar Silicon Integrated Circuits. *Proc. SPIE* **1995**, *2527*, 218.

(66) Kalluri, S.; Ziari, M.; Chen, A.; Chuyanov, V.; Steier, W. H.; Chen, D.; Jalali, B.; Fetterman, H. R.; Dalton, L. R. Monolithic Integration of Waveguide Polymer Electro-Optic Modulators on VLSI Circuitry. *IEEE Photonics Technol. Lett.* **1996**, 8, 644.

(67) Kalluri, S. Integration of Polymer Waveguide Electro-Optic Modulators with VLSI Circuits. Ph.D. Thesis, University of Southern California, Los Angeles, CA, 1997.

(68) Garner, S.; Chuyanov, V.; Chen, A.; Kalluri, S.; Marti-Carrera, F. I.; Steier, W. H.; Dalton, L. R. Three-Dimensional Integrated Optics Using Polymers. *Tech. Digest Org. Thin Films Photonic Appl., 1997 OSA Tech. Digest Ser.* **1997**, *14*, 11.

(69) Garner, S.; Chuyanov, V.; Chen, A.; Yacoubian, A.; Steier, W. H.; Dalton, L. R. Design and Fabrication of Y-Branched Vertical Power Splitters Using Polymers. *Proc. LEOS'97* **1997**, *1*, 264.

(70) Garner, S.; Chuyanov, V.; Chen, A.; Lee, S. S.; Steier, W. H.; Dalton, L. R. Integrated Optic, Vertical Polarization Splitters Using Polymers. *Proc. SPIE* **1998**, *3278*, 259.

(71) Garner, S. M.; Chuyanov, V.; Lee, S. S.; Yacoubian, A.; Chen, A.; Steier, W. H.; Wang, F.; Ren, A. S.; He, M.; Dalton, L. R. Three-Dimensional Integration of Polymer Electro-Optic Modulators. *Proc. LEOS'98* **1998**, 31.

(72) Chen, A.; Chuyanov, V.; Marti-Carrera, F. I.; Garner, S.; Steier, W. H.; Mao, S. S. H.; Ra, Y.; Dalton, L. R.; Shi, Y. Trimming of Polymer Waveguide Y-Junction by Rapid Photobleaching for Tuning the Power Splitting Ratio. *IEEE Photonics Technol. Lett.* **1997**, *9*, 1499.

(73) Chan, A.; Marti-Carrera, F. I.; Chuyanov, V.; Garner, S.; Steier, W. H.; Mao, S. S. H.; Ra, Y.; Dalton, L. R.; Shi, Y. In situ Trimming of Polymer Optical Waveguide by Rapid Photobleaching for Tuning Device Specifications. *Tech. Digest Org. Thin Films Photonic Appl., 1997 OSA Tech. Digest Ser.* **1997**, *14*, 211.

(74) Chen, A.; Chuyanov, V.; Marti-Carrera, F. I.; Garner, S.; Steier, W. H.; Dalton, L. R. Fast Trimming of Electro-Optic Polymer Waveguide Y-Branch by Post-Photobleaching for Tuning the Power Splitting Ratio. *Proc. SPIE* **1997**, *3147*, 268.

Received for review August 27, 1997
Revised manuscript received April 2, 1998
Accepted August 17, 1998

IE9705970